

## PHYSICAL CONDITIONS IN THE FOREGROUND GAS OF REFLECTION NEBULAE: NGC 2023, VDB 102, AND NGC 7023

DAVID C. KNAUTH,<sup>1</sup> S. R. FEDERMAN,<sup>1,2</sup> K. PAN, AND M. YAN  
Department of Physics and Astronomy, University of Toledo, Toledo, OH 43606

AND

DAVID L. LAMBERT  
Department of Astronomy, University of Texas at Austin, Austin, TX 78712  
*Received 2000 October 10; accepted 2001 March 6*

### ABSTRACT

High-resolution optical spectra of HD 37903 and HD 147009, which illuminate the reflection nebulae NGC 2023 and vdB 102, were obtained for comparison with our results for HD 200775 and NGC 7023. Ground-based measurements of the molecules CH, C<sub>2</sub>, and CN and the atoms Na I and K I were analyzed to extract physical conditions in the foreground cloud. Estimates of the gas density, gas temperature, and flux of ultraviolet radiation were derived and were compared with the results from infrared and radio studies of the main molecular cloud. The conditions are similar to those found in studies of diffuse clouds. The foreground material is less dense than the gas in the molecular cloud behind the star(s). The gas temperature was set at 40 K, the temperature determined for the foreground gas in NGC 7023. The flux of ultraviolet radiation was found to be less intense than in the molecular material behind the star(s). The column densities of Na I and K I were reproduced reasonably well when the extinction curve for the specific line of sight was adopted. We obtained NEWSIPS data from the *IUE* archive for HD 37903 and HD 200775. The ultraviolet data on C I and CO allow extraction of the physical conditions by alternate methods. General agreement among the various diagnostics was found, leading to self-consistent pictures of the foreground photodissociation regions.

An appendix describes checks on the usefulness of *IUE* NEWSIPS data for interstellar studies. Equivalent widths are compared with a previous analysis of *IUE* observations for interstellar gas toward 20 Aql. Excellent agreement is found with NEWSIPS results having smaller errors. A comparison of NEWSIPS data for C I toward X Per with data acquired with the *Hubble Space Telescope* shows similar levels of agreement in equivalent widths and that the derived column densities from *IUE* results are accurate to better than a factor of 2 for absorption lines of moderate strength.

*Subject headings:* ISM: atoms — ISM: individual (NGC 2023, vdB 102, NGC 7023) —  
ISM: molecules — reflection nebulae —  
stars: individual (HD 37903, HD 147009, 20 Aquilae, HD 200775)

### 1. INTRODUCTION

Stars form under the gravitational collapse of gas and dust in interstellar molecular clouds. When a newly formed star interacts with the surrounding material, the cloud's physical conditions are altered. For instance, early-type stars create photodissociation regions (PDRs), which are boundary layers between a source of far-ultraviolet (FUV) radiation and the predominantly neutral cloud (Jaffe et al. 1990). These boundaries also exist between H II regions produced by O stars and the ambient material surrounding them. In PDRs, the FUV radiation dominates the heating and chemical processes (Tielens & Hollenbach 1985a, 1985b; Hollenbach & Tielens 1999, hereafter HT99) and controls which atoms and molecules are observed. The observed relative abundances of atomic and molecular species and the use of chemical models yield the physical

conditions in the PDR. These conditions provide clues to processes that occurred immediately following star formation. In this paper we describe results for foreground PDRs in three reflection nebulae based on measurements of absorption at visible and ultraviolet wavelengths occurring at the velocity of the PDR behind the illuminating source seen via emission lines. While absorption is sometimes seen at other velocities, the main components all have velocities consistent with the molecular cloud. From this fact, we infer an association with the material behind the star.

PDRs in molecular clouds and reflection nebulae have been studied extensively at all wavelengths. Analyses have been based on measurements from X-ray to radio wavelengths. Specific observations on the nebulae studied here are given below. In an effort to obtain a comprehensive understanding of the conditions that prevail in these regions, one-dimensional, time-independent models have been developed (e.g., Tielens & Hollenbach 1985a, 1985b; van Dishoeck & Black 1986; Hollenbach, Takahashi, & Tielens 1991; Draine & Bertoldi 1996, 1999). More realistic PDR models with clumpy structure and time-dependent effects have been attempted as well (Meixner & Tielens 1993; Hollenbach & Natta 1995; Bertoldi & Draine 1996). Hollenbach & Tielens (1999) provide a comprehensive

<sup>1</sup> Guest Observer, McDonald Observatory, University of Texas at Austin.

<sup>2</sup> Visiting Astronomer, Cerro Tololo Inter-American Observatory, National Optical Astronomy Observatories, which is operated by the Association of Universities for Research in Astronomy, Inc., under cooperative agreement with the National Science Foundation; dknauth@astro1.panet.utoledo.edu.

review of observations and modeling efforts for photo-dissociation regions.

Little attention has been given to studying PDRs through atomic and molecular absorption in the visible and ultraviolet portions of the spectrum observed along the line of sight to the central or illuminating star(s). Federman et al. (1997, hereafter Paper I) analyzed visible spectra for the line of sight toward HD 200775, which illuminates the reflection nebula NGC 7023. In an effort to expand upon this work, we obtained high-resolution visible spectra toward NGC 2023 and vdB 102 as well as ultraviolet data on atoms and CO molecules in the reflection nebulae NGC 2023 and NGC 7023. The ultraviolet data were obtained from the *International Ultraviolet Explorer (IUE)* archive, which was recalibrated with the New Spectral Image Processing System (NEWSIPS). The visible and UV absorption spectra yield information about the chemical composition and the physical conditions present in the foreground PDR. A more complete picture of PDRs emerges when the physical conditions in front of the star are compared to those inferred from analyses of data obtained at other wavelengths of the main molecular cloud behind the star.

### 1.1. NGC 2023

NGC 2023 is a reflection nebula embedded in the L1630 molecular cloud (Jaffe et al. 1990) in the constellation of Orion. Infrared images of the nebula (Gatley et al. 1987; Field et al. 1994, 1998) show that it has a 6' extent with visible filamentary structures throughout and is approximately centered on the star HD 37903. In a far-infrared study, Harvey, Thronson, & Gatley (1980) showed that the molecular cloud lies behind HD 37903, which is located at a distance of 470 pc (Perryman et al. 1997). Several Herbig-Haro objects, which are associated with pre-main-sequence stars, are observed in the nebula. Two Herbig-Haro objects (HH4 and HH5) in the southeastern part of the nebula are illuminated by star C (Malin, Ogura, & Walsh 1987). Star C is thought to be a T Tauri star based on spectroscopy and its near-infrared excess. Many embedded infrared sources have also been detected (Strom et al. 1975). Wyrowski et al. (2000) detected an ultra-high-density clump ( $n \sim 10^7 \text{ cm}^{-3}$ ), which they propose could be the early stages of a protostar. Thus, NGC 2023 is an active region of star formation (Strom et al. 1975; Malin et al. 1987; Lada et al. 1991; Freyberg & Schmitt 1995).

The primary illuminating source for this nebula is HD 37903, a B1.5 V star with an effective temperature of approximately 22,000 K (Field et al. 1998). The radiation from this star has enough energy at  $\lambda \leq 912 \text{ \AA}$  to form an H II region, 0.015 pc in size, detected by radio continuum emission at the star's position within the nebula (Pankonin & Walmsley 1976, 1978; Wyrowski et al. 2000). The photons with  $\lambda \geq 912 \text{ \AA}$  create a PDR between the H II region and the rest of the neutral cloud. The proximity of the nebula and its bubble-shaped geometry (Gatley et al. 1987) make it an ideal target for studying the interaction of the UV radiation from HD 37903 with the molecular material in L1630. The reflection nebula and its PDR have been extensively studied via X-ray (Freyberg & Schmitt 1995), ultraviolet (Witt, Bohlin, & Stecher 1984, hereafter WBS84; Cardelli, Clayton, & Mathis 1989, hereafter CCM89; Buss et al. 1994), infrared (e.g., Martini, Sellgren, & DePoy 1999 and references therein), millimeter (Jaffe et al. 1990), and radio observations (Fuente, Martín-Pintado,

& Gaume 1995; Lebrón & Rodríguez 1997; Wyrowski, Walmsley, & Tielens 1997; Wyrowski et al. 2000). The studies relevant to our work will be discussed in detail later.

### 1.2. vdB 102

The central star of vdB 102 is HD 147009, an A0 V star, with an effective temperature of about 9500 K (de Geus, de Zeeuw, & Lub 1989, hereafter ddL89). This nebula was first cataloged and photometrically studied (van den Bergh 1966; Racine 1968) in the late 1960s. The nebula is 160 pc away (Perryman et al. 1997) and is one of 10 reflection nebulae in the Sco OB2 association (van den Bergh 1966; Vallée 1987; Eggen 1998). The stars in Sco OB2 illuminate different portions of the same molecular cloud. Radio observations reveal the presence of the parent molecular cloud (Kutner et al. 1980; Vallée 1987). Few observational efforts have examined the reflection nebula and its illuminating star (Chaffee & White 1982; Cappa de Nicolau & Pöppel 1986; Vallée 1987; Federman et al. 1994). For this reason, the present study greatly improves upon our knowledge of PDRs around relatively cool stars.

The remainder of the paper is organized in the following manner. In § 2 we discuss the optical and ultraviolet observations obtained for this study, as well as the consistency of our measurements with previous efforts. We describe the chemical and atomic analyses performed here and the results of these analyses as well as a comparison with our earlier results on HD 200775 (Paper I) in § 3. We discuss in § 4 the derived physical conditions and compare them with the physical conditions obtained through diagnostics at other wavelengths. Our conclusions are found in § 5. The Appendix describes checks on the usefulness of NEWSIPS data for interstellar studies such as ours.

## 2. OBSERVATIONS AND DATA REDUCTION

### 2.1. Ground-based Observations

#### 2.1.1. McDonald 2dcoudé Data

High-resolution echelle spectra of HD 37903, HD 147009, and 20 Aql were taken with the 2.7 m telescope of the University of Texas McDonald Observatory during 1996 June, 1997 July, and 1998 January. Observations of 20 Aql were made since it allows for the comparison of our optical data with others and is located behind a relatively isolated cloud for an additional test of the atomic analysis discussed below. The “2dcoudé” spectrograph (Tull et al. 1995) was used with two camera setups, and a Tektronix charge-coupled device (CCD) was the detector. One camera provided high spectral resolution with a resolving power at 4000 Å of  $R \approx 180,000$  ( $\Delta v \approx 2 \text{ km s}^{-1}$ ) and covered the wavelength range 3800–4400 Å. This high-resolution mode yielded spectra containing eight disjoint echelle orders approximately 15 Å wide, separated by approximately 65 Å. This setup provided spectra on the following interstellar species CH<sup>+</sup>, CH, CN, Ca II K, and Ca I. The second camera setting resulted in moderate spectral resolution with a resolving power at 7000 Å of  $R \approx 52,000$  ( $\Delta v \approx 6 \text{ km s}^{-1}$ ) and covered the wavelength range 3600–9700 Å. The moderate-resolution spectra consisted of 59 orders with an overlap of about 15 Å at the blue end. The interorder separation increased with wavelength until there was approximately 150 Å between orders at near-infrared wavelengths. In addition to observing the same species obtained from the high-resolution spectra, we also obtained data on

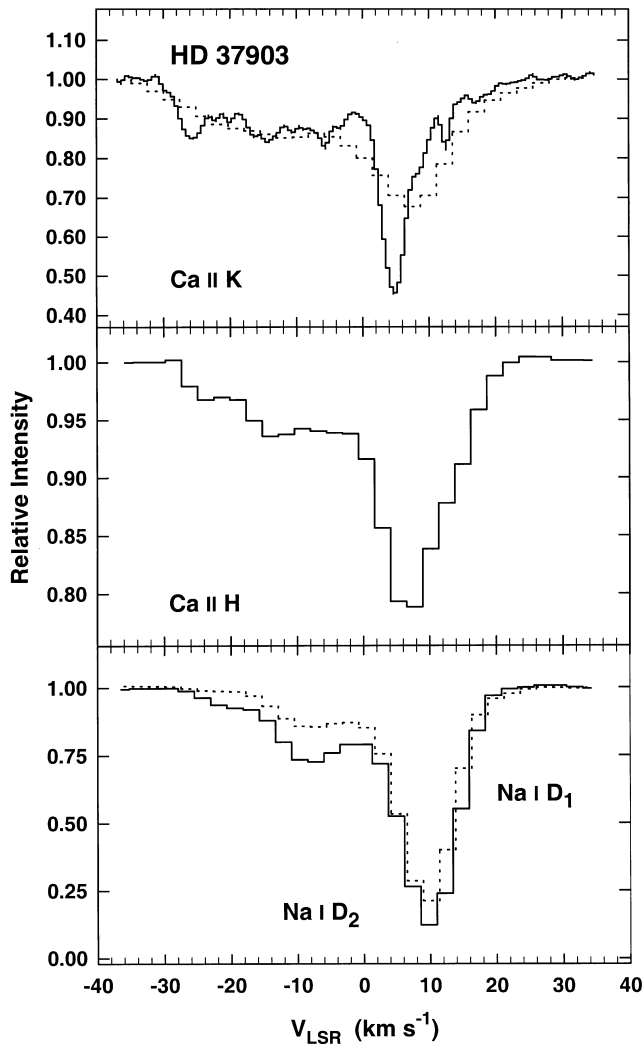


FIG. 1.—Representative interstellar atomic spectra toward HD 37903. *Top*: Ca II K; solid line is high-resolution 2dcoudé data, and dashed line is moderate-resolution 2dcoudé data. In all figures the flux is normalized to unity. There is a nice correspondence between the two different resolutions in velocity and line shape. *Middle*: Moderate-resolution 2dcoudé Ca II H data. *Bottom*: Moderate-resolution 2dcoudé data; dashed line is Na I D<sub>1</sub>, and solid line is Na I D<sub>2</sub>. The slight velocity differences are attributed to an error in wavelength solution.

Ca II H, Na I D<sub>1</sub>, K I, and C<sub>2</sub>. The resolution was determined from the FWHM of Thorium-Argon (Th-Ar) lines.

The data were reduced in a standard way utilizing the NOAO SUN/IRAF software (Revision 2.10.4). Dark, bias, and flat lamp exposures were taken each night to remove any instrumental effects due to the CCD detector. Comparison spectra were taken periodically throughout the night, typically every 2 hr. The average bias exposure was subtracted from all raw stellar, comparison (Th-Ar), and flat images. The scattered light was fitted by a low-order polynomial, in both the dispersion direction and perpendicular to it for the multiorder observations, and removed. The pixel-to-pixel sensitivity was removed by dividing the normalized average flat into the stellar spectra. Next, the pixels perpendicular to the dispersion were summed in each order for each stellar and comparison lamp exposure. The extracted spectra were placed on an appropriate wavelength scale with the Th-Ar comparison spectra and

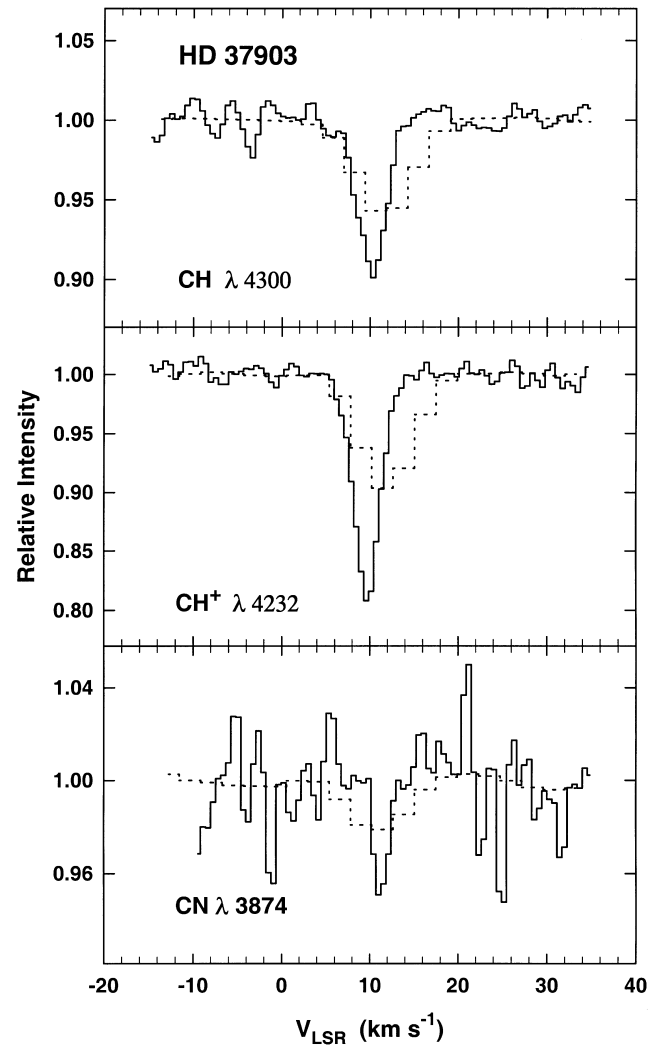


FIG. 2.—Representative interstellar molecular spectra toward HD 37903. *Top*: CH; solid line is high-resolution 2dcoudé data, and dashed line is moderate-resolution 2dcoudé data. *Middle*: CH<sup>+</sup>; same as top panel. *Bottom*: CN; same as top panel. There is a general agreement in velocity and line shape; the slight velocity differences are attributed to an error in wavelength solution.

Doppler corrected. The spectra were co-added and normalized to unity yielding a final spectrum with high signal-to-noise ratio (based on the rms deviations in the continuum), typically 100:1.

### 2.1.2. McDonald Observations with the 6 Foot Camera

The 6 foot camera of the coude spectrograph on the 2.7 m telescope was used to acquire high-resolution spectra of HD 147009 and 20 Aql. Observations, at  $R \approx 200,000$ , of interstellar Na I D  $\lambda\lambda 5896, 5890$ , K I  $\lambda 7699$ , CH<sup>+</sup>  $\lambda 4232$ , and Ca I  $\lambda 4226$  were obtained in 1990 June, Ca II K  $\lambda 3933$  observations were made in 1991 June, and CH  $\lambda 4300$  observations were obtained in 1992 June. The TI2 CCD with 15  $\mu\text{m}$  pixels was used in all setups. Since no cross disperser was used, single orders of the echelle grating were detected in the vicinity of the line of interest. Appropriate interference filters were placed at the entrance slit to remove light from unwanted orders. Scattered light was

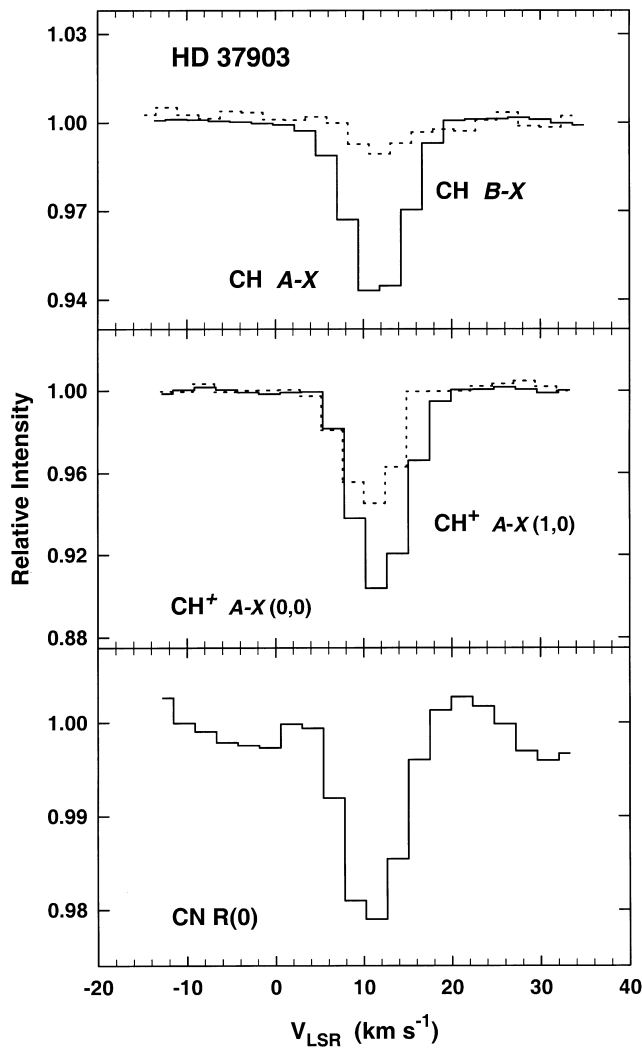


FIG. 3.—Moderate-resolution 2dcoudé molecular spectra toward HD 37903. *Top*: CH; solid line is  $A-X$  transition, and dashed line is  $B-X$  transition. *Middle*:  $CH^+$ ; solid line is  $A-X(0-0)$  transition, and dashed line is  $A-X(1-0)$  transition. *Bottom*: CN  $R(0)$  transition is shown.

found to be negligible since only one order was observed. Comparison spectra from a Th-Ar hollow cathode were taken throughout the night, while biases and flat fields were acquired each night. Dark frames were also obtained as a check on the amount of thermal noise from the cooled CCD. The slit was imaged onto 2.5 pixels for all setups, providing a resolution of  $1.6\text{--}1.8\text{ km s}^{-1}$ . The data were reduced in the standard manner described above. The resulting signal-to-noise ratios ranged from 30 to 200.

### 2.1.3. Cerro Tololo Inter-American Observatory (CTIO) Observations

The stars HD 147009 and 20 Aql were observed with the Bench Mounted Echelle on the 1.5 m telescope in 1991 July. The setup involved the 590 mm long camera, the Ritchey Chrétien grating from the 4 m telescope as a cross disperser, the TI1  $800 \times 800$  pixel CCD, and a  $\text{CuSO}_4$  blocking filter. The entrance slit at the end of the  $200\text{ }\mu\text{m}$  fiber optic feed was set at  $45\text{ }\mu\text{m}$ , illuminating 2.6 pixels as determined by the FWHM of Th-Ar lines. The resulting instrumental resolving power was about 65,000. The setup allowed measurement of lines between 3800 and 4400 Å. Bias frames and

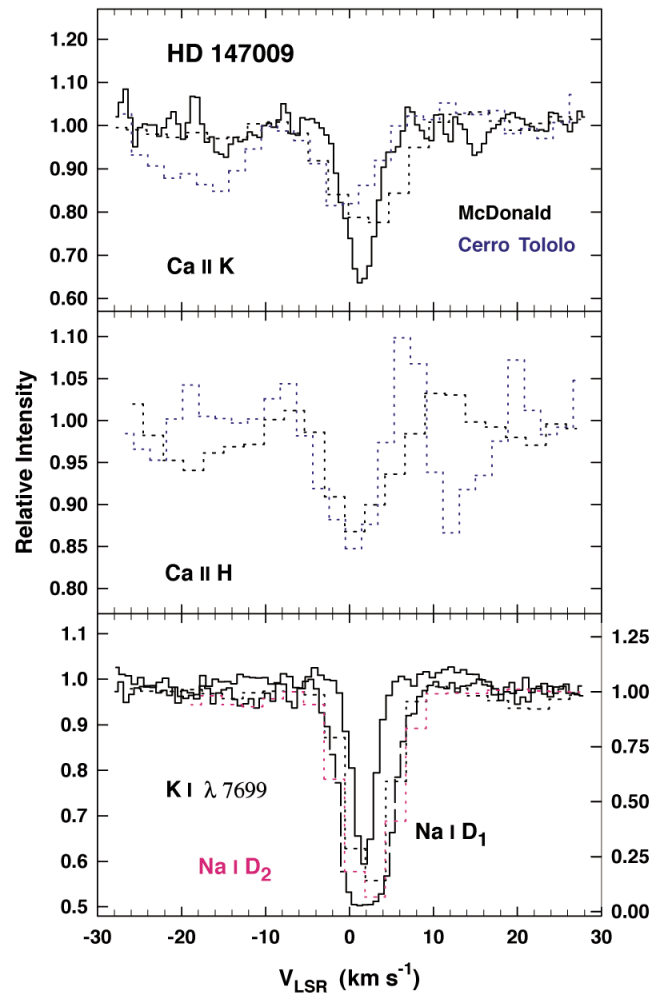


FIG. 4.—Representative interstellar atomic spectra toward HD 147009. *Top*: Ca II K; thick solid line is high-resolution 2dcoudé data, thick dashed line is moderate-resolution 2dcoudé data, and blue dashed line is moderate-resolution CTIO data. *Middle*: Ca II H; thick dashed line is moderate-resolution 2dcoudé data, and blue dashed line is moderate-resolution CTIO data. Apparent minimum in the CTIO data is noise, not an additional component. *Bottom*: Spectra of several atomic species taken with different instruments at different resolutions. There is excellent agreement among all observations. The solid line is K I and the thick long-dashed line is Na I  $D_1$ , high-resolution 6 foot camera data, thick dashed line is moderate-resolution 2dcoudé Na  $D_1$  data, and pink dashed line is moderate-resolution 2dcoudé Na  $D_2$  data. Use the left scale for K I and the right scale for Na I  $D$  lines.

flat fields were acquired each night. The wavelength scale was determined from spectra of a Th-Ar hollow cathode taken throughout the night. The data were reduced in the standard manner described above. The extracted spectra had signal-to-noise ratios between 40 and 150.

A sample of the rectified ground-based spectra for atoms and molecules toward HD 37903 is shown in Figures 1–3, and Figures 4–6 exhibit spectra of HD 147009. The equivalent width,  $W_\lambda$ , for a line was determined by a Gaussian fit; single Gaussians were adequate for all except the atomic species Na I and Ca II toward HD 37903. The measured equivalent widths and  $v_{\text{LSR}}$  for the ground-based results toward HD 37903 and HD 147009 are shown in Tables 1–3. Where applicable, measurements taken from the literature are also shown. All  $W_\lambda$  values for a given line agree within measured uncertainties. The differences in  $v_{\text{LSR}}$  are attrib-

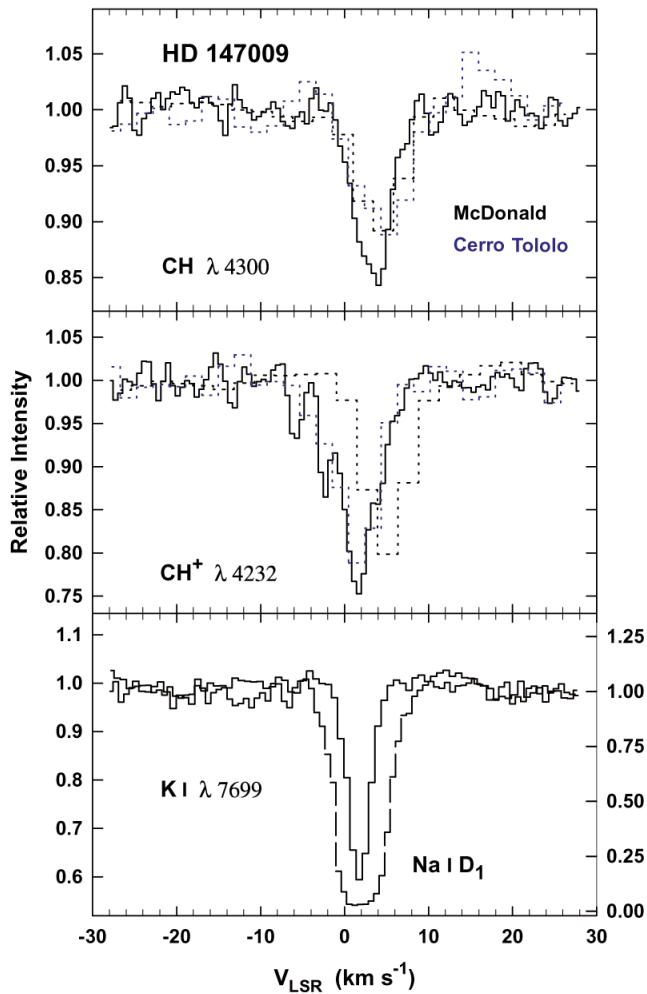


FIG. 5.—Representative interstellar spectra toward HD 147009 are shown. *Top*: CH; thick solid line is high-resolution 2dcoudé data, thick dashed line is moderate-resolution 2dcoudé data, and blue dashed line is moderate-resolution CTIO data. *Middle*: CH<sup>+</sup>; solid line is high-resolution 2dcoudé data, thick dashed line is moderate-resolution 2dcoudé data, and blue dashed line is moderate-resolution CTIO data. The slight velocity differences are attributed to an error in wavelength solution. *Bottom*: Spectra of K I (solid line, left scale) and Na I D<sub>1</sub> (dashed line, right scale), taken with the high-resolution 6 foot camera.

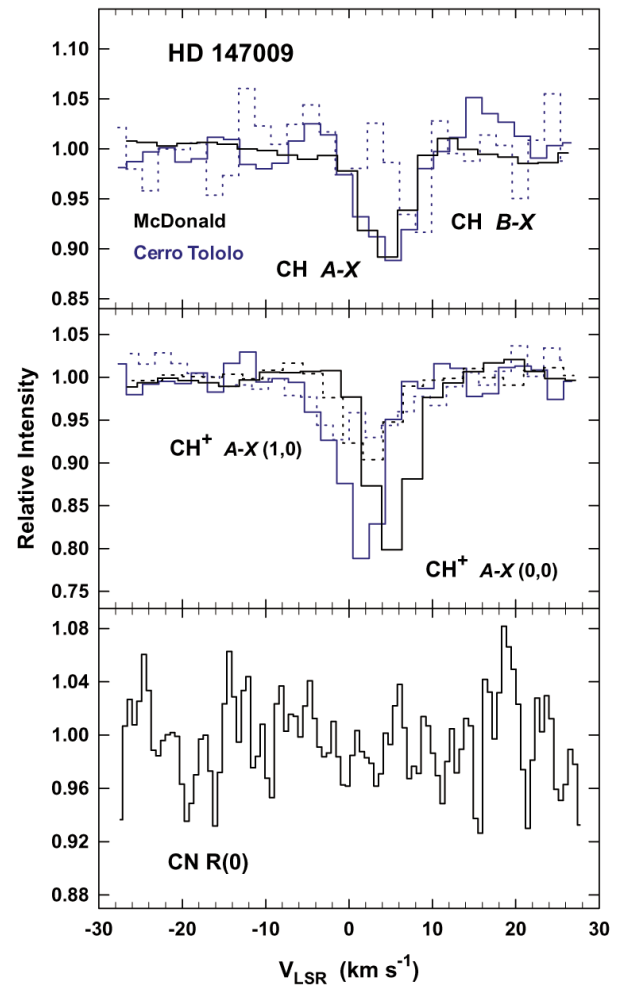


FIG. 6.—Interstellar molecular spectra toward HD 147009; thick lines are 2dcoudé data, and blue lines are CTIO data. *Top*: CH; the solid lines are the A-X transition, and the dashed line is the B-X transition. *Middle*: CH<sup>+</sup>; the solid lines are the A-X (0-0) transition, and the dashed lines are the A-X (1-0) transition. The slight velocity differences are attributed to an error in wavelength solution in these moderate-resolution data. *Bottom*: High-resolution 2dcoudé 3874 Å region of the spectrum where CN resides; no detection is evident.

uted to differences in spectral resolution and to systematic effects involving the wavelength solution. Where no interstellar absorption was detected, a  $3\sigma$  upper limit is given.

Each  $W_\lambda$  was converted into a column density utilizing curves of growth. The column densities for each species were consistent within the errors from individual measurements. The final column densities reported in Tables 4 and 5 for HD 37903 and HD 147009, respectively, are the weighted average of all detections reported in this work and the literature. For the C<sub>2</sub> results reported in Table 3, the most restrictive upper limits for a rotational level were summed to get the total upper limit in column density.

The Doppler parameter ( $b$ -value) was set at  $1 \text{ km s}^{-1}$  for all lines except those of Ca II and CH<sup>+</sup>, where a  $b$ -value of  $2.5 \text{ km s}^{-1}$  was used (e.g., Welty, Morton, & Hobbs 1996). For Na I and K I absorption associated with the molecular material of the PDR,  $b$ -values of  $2.0 \text{ km s}^{-1}$  toward HD 37903 and  $1.5 \text{ km s}^{-1}$  toward HD 147009 were required by the atomic analysis discussed below. These

$b$ -values are similar to other sight lines studied in Orion and the Sco OB2 association based on high-resolution surveys of interstellar Na I D<sub>1</sub> and K I (Welty, Hobbs, & Kulkarni 1994; Welty & Hobbs 2001). The change in  $b$ -value affected only the column of Na I since the optical depth at line center is larger for Na I than for K I. This resulted in a 20% decrease in  $N(\text{Na I})$  toward HD 37903 and a 10% decrease toward HD 147009; no change in  $N(\text{K I})$  occurred with the change in  $b$ -value.

## 2.2. Ultraviolet Data

High-resolution ultraviolet spectra of HD 37903 and HD 200775 were available in the IUE NEWSIPS archive. Table 6 lists the short-wavelength spectral images used in our study. The data were extracted with the set of programs in IUERDAF. For features that appeared in two orders, the cleaner looking spectrum was used for further analysis. Once extracted, the spectra were analyzed with the IRAF package in much the same way as described

TABLE 1  
 COMPILATION OF GROUND-BASED RESULTS FOR HD 37903

SPECIES	WAVELENGTH (Å)	MCD (MODERATE RES) <sup>a</sup>		MCD (HIGH RES) <sup>a</sup>		OTHER	
		$W_{\lambda}$ (mÅ)	$v_{\text{LSR}}$ (km s <sup>-1</sup> )	$W_{\lambda}$ (mÅ)	$v_{\text{LSR}}$ (km s <sup>-1</sup> )	$W_{\lambda}$ (mÅ)	$v_{\text{LSR}}$ (km s <sup>-1</sup> )
CH .....	4300.313	7.0±0.1	11.7	5.9±0.4	10.3	≤7.8 <sup>b</sup>	...
		...	...	...	...	≤12.5 <sup>c</sup>	...
		...	...	...	...	6.4±0.3 <sup>d</sup>	10.0
		...	...	...	...	...	...
		...	...	...	...	...	...
CH <sup>+</sup> .....	4232.548	10.7±0.1	11.8	9.8±0.3	9.7	10.7±2.4 <sup>c</sup>	7.4
		...	...	...	...	10.8±0.5 <sup>d</sup>	9.1
		...	...	...	...	≤16.0 <sup>c</sup>	...
		...	...	...	...	5.3±0.8 <sup>d</sup>	10.1
		...	...	...	...	...	...
CN .....	3874.00	0.7±0.3	9.3	≤2.5	...	...	...
		...	...	...	...	...	...
		...	...	...	...	...	...
Ca II .....	3968.468	3.2±0.3	-22.9	...	...	...	...
		...	...	...	...	...	...
Ca II .....	3933.663	8.8±0.4	-13.0	...	...	...	...
		10.8±0.5	-1.6	...	...	...	...
		18.0±0.3	6.2	...	...	19.7±5.0 <sup>d</sup>	6.4
		9.3±0.3	11.5	...	...	...	...
		3.5±0.2	16.0	...	...	...	...
		12.8±0.6	-23.0	11.8±0.9	-25.4	...	...
		20.7±0.6	-14.0	22.8±1.5	-15.5	...	...
		20.3±0.6	-3.3	17.8±1.5	-4.8	...	...
		33.6±0.5	5.9	31.3±0.7	4.3	...	...
		15.4±0.4	11.2	16.3±1.1	9.7	...	...
Ca I .....	4226.728	7.5±0.5	18.8	6.7±1.3	17.3	...	...
		1.3±0.4	8.8	≤1.1	...	≤10.0 <sup>c</sup>	...
Na I .....	5895.924	...	...	...	...	≤1.5 <sup>d</sup>	...
		2.1±3.0	-20.7	...	...	...	...
		18.7±3.0	-10.5	...	...	...	...
		17.6±3.0	-4.3	...	...	...	...
		21.8±3.3	3.9	...	...	...	...
K I .....	7698.974	140.6±3.3	10.0	...	...	...	...
		4.7±2.2	19.7	...	...	...	...
		...	...	...	...	18.8 <sup>e</sup>	10

<sup>a</sup> 2dcoudé.  
<sup>b</sup> Federman et al. 1994.  
<sup>c</sup> Allen 1994.  
<sup>d</sup> Gredel, van Dishoeck, & Black 1993.  
<sup>e</sup> D. E. Welty 2000, private communication.

TABLE 2  
 COMPILATION OF GROUND-BASED RESULTS FOR HD 147009

SPECIES	WAVELENGTH (Å)	MCD (MODERATE RES) <sup>a</sup>		MCD (HIGH RES) <sup>a</sup>		MCD (HIGH RES) <sup>b</sup>		CTIO (MODERATE RES)		OTHER
		$W_{\lambda}$ (mÅ)	$v_{\text{LSR}}$ (km s <sup>-1</sup> )	$W_{\lambda}$ (mÅ)	$v_{\text{LSR}}$ (km s <sup>-1</sup> )	$W_{\lambda}$ (mÅ)	$v_{\text{LSR}}$ (km s <sup>-1</sup> )	$W_{\lambda}$ (mÅ)	$v_{\text{LSR}}$ (km s <sup>-1</sup> )	$W_{\lambda}$ (mÅ)
CH .....	4300.313	10.4±0.5	4.3	11.6±0.8	4.0	...	...	12.3±1.5	-0.9	8.8±2.8 <sup>c</sup>
		...	...	...	...	...	...	...	...	...
		...	...	...	...	...	...	...	...	...
		...	...	...	...	...	...	...	...	...
CH <sup>+</sup> .....	4232.548	18.0±0.7	5.1	19.6±1.4	1.6	...	...	19.0±1.4	1.8	...
		...	...	...	...	...	...	...	...	...
CN .....	3874.00	...	...	...	...	...	...	...	...	...
		...	...	...	...	...	...	...	...	...
		...	...	...	...	...	...	...	...	...
Ca II .....	3968.468	13.6±2.9	1.0	...	...	...	...	...	...	...
		...	...	...	...	...	...	...	...	...
Ca II .....	3933.663	29.2±1.6	2.1	22.4±2.3	1.4	...	...	20.1±3.2	-0.9	...
		...	...	...	...	...	...	...	...	...
Ca I .....	4226.728	≤2.6	...	≤0.9	...	...	...	≤2.2	...	...
Na I .....	5895.924	111.3±5.4	2.5	...	...	137.0±4.0	1.2	...	...	...
K I .....	7698.974	42.3±4.0	2.7	...	...	33.0±1.0	1.6	...	...	...

<sup>a</sup> 2dcoudé.  
<sup>b</sup> 6 foot camera.  
<sup>c</sup> Federman et al. 1994.

TABLE 3  
 C<sub>2</sub> RESULTS

LINE	WAVELENGTH (Å)	HD 37903		HD 147009	
		$W_{\lambda}$ (mÅ)	$N^a$ (cm <sup>-2</sup> )	$W_{\lambda}$ (mÅ)	$N^a$ (cm <sup>-2</sup> )
R(0).....	8757.69	≤1.5	≤2.2 × 10 <sup>12</sup>	≤2.9	≤4.4 × 10 <sup>12</sup>
P(2).....	8766.03	≤1.2	≤1.8 × 10 <sup>13</sup>	≤2.1	≤3.1 × 10 <sup>13</sup>
Q(2).....	8761.19	≤0.6	≤1.8 × 10 <sup>12</sup>	≤2.2	≤6.6 × 10 <sup>12</sup>
R(2).....	8753.95	≤0.6	≤2.3 × 10 <sup>12</sup>	≤3.2	≤1.2 × 10 <sup>13</sup>
P(4).....	8773.43	≤0.6	≤5.6 × 10 <sup>13</sup>	≤2.1	≤1.9 × 10 <sup>13</sup>
Q(4).....	8763.75	≤0.8	≤2.4 × 10 <sup>12</sup>	≤2.1	≤6.3 × 10 <sup>12</sup>
R(4).....	8751.68	≤0.4	≤2.0 × 10 <sup>12</sup>	≤1.7	≤7.8 × 10 <sup>12</sup>
P(6).....	8782.31	≤1.2	≤9.2 × 10 <sup>12</sup>	≤3.6	≤2.8 × 10 <sup>13</sup>
Q(6).....	8767.76	≤1.0	≤3.0 × 10 <sup>12</sup>	≤2.7	≤8.1 × 10 <sup>12</sup>
R(6).....	8750.85	≤0.4	≤2.1 × 10 <sup>12</sup>	≤1.7	≤8.5 × 10 <sup>12</sup>
Q(8).....	8773.22	≤0.6	≤1.9 × 10 <sup>12</sup>	≤2.9	≤8.7 × 10 <sup>12</sup>
$N_{\text{tot}}(\text{C}_2)$ .....	...	...	≤9.9 × 10 <sup>12</sup>	...	≤3.4 × 10 <sup>13</sup>

<sup>a</sup>  $b = 1.0 \text{ km s}^{-1}$ .

 TABLE 4  
 COLUMN DENSITIES FOR HD 37903

Species	Wavelength (Å)	$v_{\text{LSR}}$ (km s <sup>-1</sup> )	$N_{\text{obs}}^{\text{a,b}}$ (cm <sup>-2</sup> )
$N(\text{CH})$ .....	4300.313	10.7	$(9.2 \pm 0.1) \times 10^{12}$
	3878.774	...	≤4.1 × 10 <sup>12</sup>
	3886.409	11.8	$(2.5 \pm 0.7) \times 10^{12}$
	3890.217	...	≤9.6 × 10 <sup>12</sup>
$N_{\text{tot}}(\text{CH})$ .....	...	...	$(9.2 \pm 0.1) \times 10^{12}$
$N(\text{CH}^+)$ .....	4232.548	9.2	$(1.3 \pm 0.1) \times 10^{13}$
	3957.692	10.4	$(1.2 \pm 0.1) \times 10^{13}$
$N_{\text{tot}}(\text{CH}^+)$ .....	...	...	$(1.3 \pm 0.1) \times 10^{13}$
$N(\text{CN})$ .....	3874.00	9.3	$(2.3 \pm 1.0) \times 10^{11}$
	3874.61	10.1	$(5.6 \pm 0.9) \times 10^{11}$
	3875.76	...	≤8.8 × 10 <sup>11</sup>
$N_{\text{tot}}(\text{CN})$ .....	...	...	$(7.9 \pm 1.5) \times 10^{11}$
$N(\text{Ca II H})$ .....	3968.468	-22.9	$(7.4 \pm 0.7) \times 10^{10}$
$N(\text{Ca II K})$ .....	3933.663	-25.4	$(1.6 \pm 0.1) \times 10^{11}$
$N_{-2.5}(\text{Ca II})$ .....	...	...	$(1.2 \pm 0.1) \times 10^{11}$
$N(\text{Ca II H})$ .....	3968.468	-13.0	$(2.1 \pm 0.1) \times 10^{11}$
$N(\text{Ca II K})$ .....	3933.663	-14.7	$(2.8 \pm 0.1) \times 10^{11}$
$N_{-1.5}(\text{Ca II})$ .....	...	...	$(2.5 \pm 0.1) \times 10^{11}$
$N(\text{Ca II H})$ .....	3968.468	-1.6	$(2.6 \pm 0.1) \times 10^{11}$
$N(\text{Ca II K})$ .....	3933.663	-3.3	$(2.6 \pm 0.1) \times 10^{11}$
$N_{-2}(\text{Ca II})$ .....	...	...	$(2.6 \pm 0.1) \times 10^{11}$
$N(\text{Ca II H})$ .....	3968.468	6.2	$(4.6 \pm 0.1) \times 10^{11}$
$N(\text{Ca II K})$ .....	3933.663	5.1	$(4.8 \pm 0.1) \times 10^{11}$
$N_{+5}(\text{Ca II})$ .....	...	...	$(4.7 \pm 0.1) \times 10^{11}$
$N(\text{Ca II H})$ .....	3968.468	11.5	$(2.3 \pm 0.1) \times 10^{11}$
$N(\text{Ca II K})$ .....	3933.663	10.5	$(2.0 \pm 0.1) \times 10^{11}$
$N_{+10}(\text{Ca II})$ .....	...	...	$(2.1 \pm 0.1) \times 10^{11}$
$N(\text{Ca II H})$ .....	3968.468	16.0	$(8.2 \pm 0.5) \times 10^{10}$
$N(\text{Ca II K})$ .....	3933.663	18.1	$(8.9 \pm 0.6) \times 10^{10}$
$N_{+18}(\text{Ca II})$ .....	...	...	$(8.5 \pm 0.4) \times 10^{10}$
$N_{\text{tot}}(\text{Ca I})$ .....	4226.728	8.8	$(4.8 \pm 1.5) \times 10^9$
$N_{-2.5}(\text{Na I})$ .....	5895.924	-20.7	$(2.2 \pm 2.7) \times 10^{10}$
$N_{-10}(\text{Na I})$ .....	...	-10.5	$(2.2 \pm 0.4) \times 10^{11}$
$N_{-5}(\text{Na I})$ .....	...	-4.3	$(2.1 \pm 0.4) \times 10^{11}$
$N_{+4}(\text{Na I})$ .....	...	3.9	$(2.6 \pm 0.5) \times 10^{11}$
$N_{+10}(\text{Na I})$ .....	...	10.0	$(1.1 \pm 0.2) \times 10^{13}$
$N_{+20}(\text{Na I})$ .....	...	19.7	$(5.0 \pm 0.7) \times 10^{10}$
$N_{\text{tot}}(\text{K I})$ .....	7698.974	10	$1.1 \times 10^{11 \text{ c}}$

<sup>a</sup> Column densities determined from weighted average of detections.

<sup>b</sup>  $b = 1.0 \text{ km s}^{-1}$  for CH, CN, and Ca I; 2.5 km s<sup>-1</sup> for CH<sup>+</sup> and Ca II; and 2.0 km s<sup>-1</sup> for Na I and K I.

<sup>c</sup> D. E. Welty 2000, private communication.

above for the ground-based measurements. Our focus was on absorption from <sup>12</sup>CO, <sup>13</sup>CO, C I, S I, and Ni II; sample spectra are shown in Figures 7 and 8. Since C I and S I represent minor constituents for their respective elements and have similar ionization potentials, the S I lines provided a check on the C I lines. On the other hand, Ni II is the dominant form of Ni in cloud envelopes; the synthesis of Ni II lines allowed for a comparison of  $b$ -values that could elucidate the relative volumes occupied by dominant versus minor forms of an element.

The compilation of  $W_{\lambda}$  values appears in Table 7. Joseph et al. (1986) reported results for HD 37903 from the same *IUE* spectra, but with an earlier version of the archiving process. The overall agreement between the two sets of  $W_{\lambda}$  is good; the NEWSIPS data used here produce spectra with higher signal-to-noise ratio, as seen by the smaller uncertainties in  $W_{\lambda}$ . We performed several checks on  $W_{\lambda}$  values measured from NEWSIPS spectra; these are described in

 TABLE 5  
 COLUMN DENSITIES FOR HD 147009

Species	Wavelength (Å)	$v_{\text{LSR}}$ (km s <sup>-1</sup> )	$N_{\text{obs}}^{\text{a,b}}$ (cm <sup>-2</sup> )
$N(\text{CH})$ .....	4300.313	4.1	$(1.5 \pm 0.1) \times 10^{13}$
	3878.774	...	≤3.3 × 10 <sup>13</sup>
	3886.409	...	≤1.9 × 10 <sup>13</sup>
	3890.217	...	≤4.4 × 10 <sup>13</sup>
$N_{\text{tot}}(\text{CH})$ .....	...	...	$(1.5 \pm 0.1) \times 10^{13}$
$N(\text{CH}^+)$ .....	4232.548	2.8	$(2.4 \pm 0.1) \times 10^{13}$
	3957.692	2.4	$(2.0 \pm 0.2) \times 10^{13}$
$N_{\text{tot}}(\text{CH}^+)$ .....	...	...	$(2.3 \pm 0.1) \times 10^{13}$
$N(\text{CN})$ .....	3874.61	...	≤5.5 × 10 <sup>11</sup>
$N_{\text{tot}}(\text{CN})$ .....	...	...	≤8.3 × 10 <sup>11</sup>
$N(\text{Ca II H})$ .....	3968.468	1.0	$(3.4 \pm 0.8) \times 10^{11}$
$N(\text{Ca II K})$ .....	3933.663	1.8	$(3.3 \pm 0.2) \times 10^{11}$
$N_{\text{tot}}(\text{Ca II})$ .....	...	...	$(3.3 \pm 0.2) \times 10^{11}$
$N_{\text{tot}}(\text{Ca I})$ .....	4226.728	...	≤3.2 × 10 <sup>9</sup>
$N_{\text{tot}}(\text{Na I})$ .....	...	1.9	$(1.5 \pm 0.3) \times 10^{13}$
$N_{\text{tot}}(\text{K I})$ .....	7698.974	2.2	$(2.3 \pm 0.1) \times 10^{11}$

<sup>a</sup> Column densities determined from weighted average of detections.

<sup>b</sup>  $b = 1.0 \text{ km s}^{-1}$  for CH, CN, and Ca I; 2.5 km s<sup>-1</sup> for CH<sup>+</sup> and Ca II; and 1.5 km s<sup>-1</sup> for Na I and K I.

TABLE 6  
IUE ARCHIVE FILES

Star	$V$	Spectral Type	$(B-V)_s$	$E(B-V)$	Image Number	Notes
HD 31726 .....	6.15	B1 V	-0.21	0.05	SWP 8165; LWR 7098	a
HD 37023 .....	6.70	B0.5 Vp	0.09	0.37	SWP 4281; LWR 3782	b
HD 37903 .....	7.82	B1.5 V	0.07	0.35	SWP 6953, 8058, 8055, 8057, 21293-4; LWR 7025	b, c, d
HD 55857 .....	6.11	B0.5 V	-0.26	0.02	SWP 14339; LWR 10953	e
HD 64802 .....	5.49	B2 V	-0.19	0.05	SWP 14308; LWR 10939	a
HD 147009 .....	8.05	A0 V	0.26	0.38	SWP 22733-4; LWR 17366-7	b
$\zeta$ Aql .....	2.99	A0 V	0.01	0.01	SWP 8269-70; LWR 7292-4	c, f
20 Aql .....	5.37	B3 V	0.09	0.33	SWP 8974, 8976, 13865, 36939-40	d
HD 200775 .....	7.20	B2 Ve	0.34	0.45	SWP 9836-7, 25734, 54089	d

<sup>a</sup> Unreddened star spectra, average of the two used as comparison for HD 37903 (Fitzpatrick & Massa 1990).

<sup>b</sup> Reddened star spectra used for extinction curves (Fitzpatrick & Massa 1990).

<sup>c</sup> Witt et al. 1981.

<sup>d</sup> NEWSIPS data used for UV analysis.

<sup>e</sup> Unreddened star spectra used as comparison for HD 37023 (Fitzpatrick & Massa 1990).

<sup>f</sup> Unreddened star spectra used as comparison for HD 147009.

the Appendix. For the features considered in our study, we are confident that they have been measured reliably.

Profile synthesis was used to extract  $b$ -values and column densities from the spectra. A  $\chi^2$  minimization procedure was adopted for the fits. The syntheses were based on the following set of oscillator strengths: Morton & Noreau (1994) for  $^{12}\text{CO}$  and  $^{13}\text{CO}$ ; Morton (1991) and Zsargó, Federman, & Cardelli (1997) for C I; Federman & Cardelli (1995) for S I; and Morton (1991) and Zsargó & Federman (1998) for Ni II. The resulting column densities appear in Table 8. For the synthesis of the CO bands, the excitation temperature was set at 4 K (Lambert et al. 1994) and the  $b$ -value was found to be somewhat less than  $1 \text{ km s}^{-1}$ . For the atomic lines, the  $b$ -value was determined by fits to several lines. There was no discernible difference in  $b$ -value

between neutral atoms and ions; we found  $b = 2.0 \pm 0.5 \text{ km s}^{-1}$ . Since CO is expected to occupy a more restricted volume than even neutral atoms, a smaller  $b$ -value for this species is appropriate.

### 3. ANALYSIS AND RESULTS

#### 3.1. Chemical Modeling

The chemistry of the simple molecular species CH,  $\text{C}_2$ , and CN is relatively well understood (van Dishoeck & Black 1986; Federman et al. 1994), and relevant reaction rates are known or have been calculated. The purpose of obtaining data on several species of carbon-bearing molecules is to glean information about the physical conditions where these species reside. In particular, gas density ( $n$ ), gas

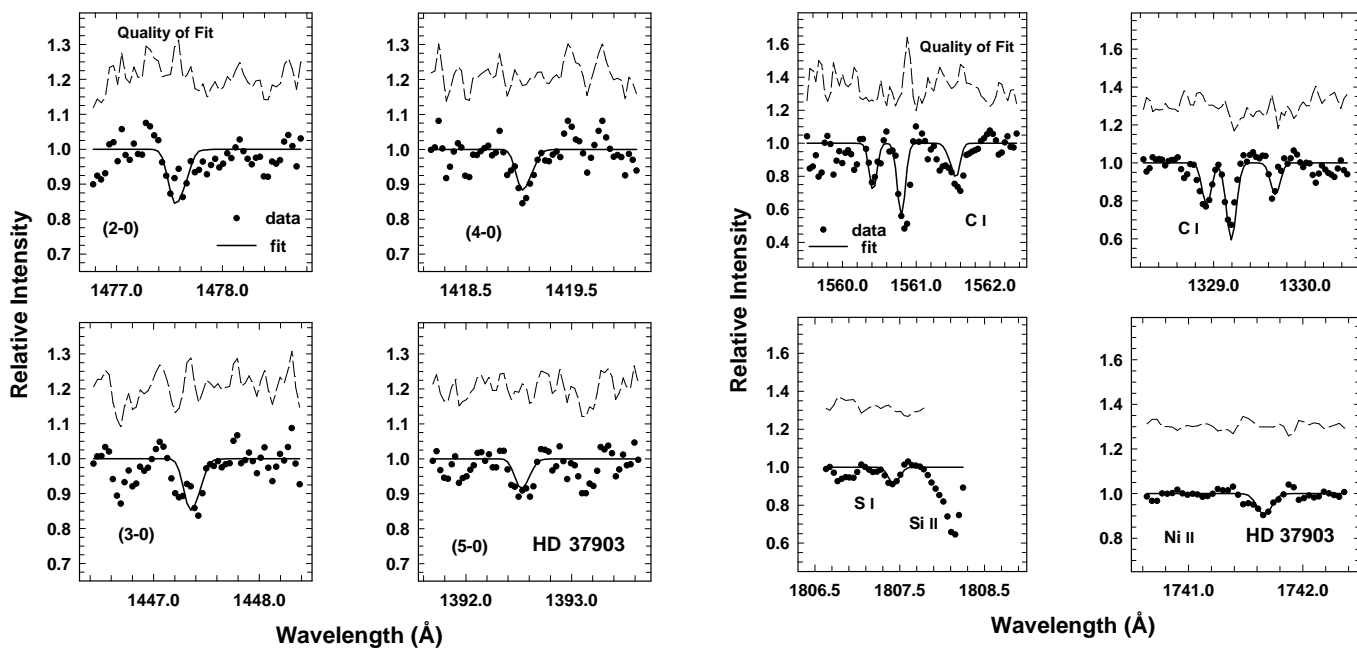


Fig. 7a

Fig. 7b

FIG. 7.—(a) Representative NEWSIPS IUE  $^{12}\text{CO}$  spectra toward HD 37903. The data are represented by the filled circles. Our best fit to the data (solid line) and the data - fit (dashed line, offset to 1.22) are also shown. (b) Same as (a), but with spectra of C I, S I, and Ni II. The Si II line was not fitted. Data fit offset to 1.30.



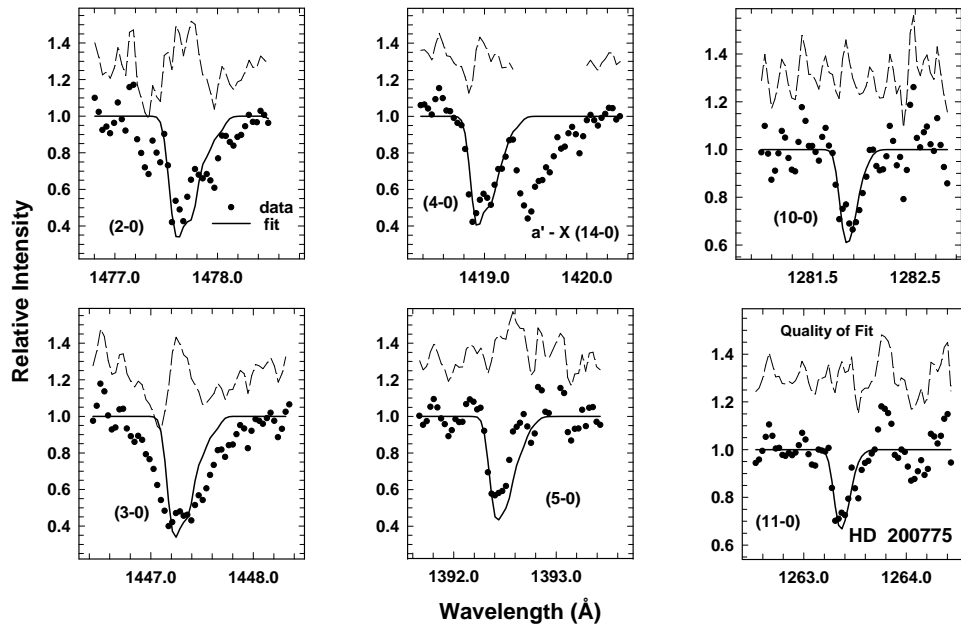


Fig. 8a

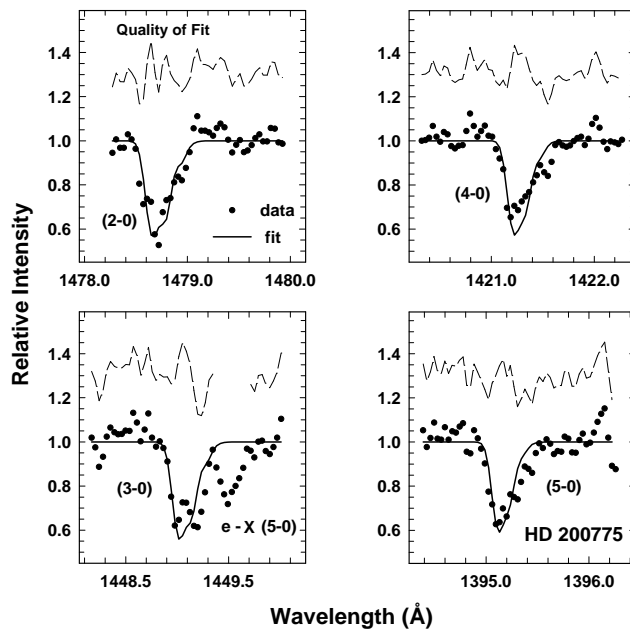


Fig. 8b

FIG. 8.—(a) Representative NEWSIPS  $IUE$   $^{12}\text{CO}$  spectra toward HD 200775. The data are represented by the filled circles. Our best fit to the data (solid line) and the data — fit (dashed line, offset to 1.30) are also shown. The  $a'-X$  (14-0) intersystem band was not fitted. (b) Same as (a), but with spectra of  $^{13}\text{CO}$ . The  $e-X$  (5-0) band of  $^{12}\text{CO}$  is clearly seen in the spectrum as well. (c) Same as (a), but with spectra of C I, S I and Ni II. The Si II line was not fitted.

temperature ( $T$ ), and the enhancement of the ultraviolet flux over the average interstellar value given by Draine (1978),  $I_{\text{UV}}$ , can be extracted from the measurements.

The analysis is based on steady state chemical rate equations, which were successful in reproducing data for quiescent diffuse interstellar clouds (e.g., Federman et al. 1994) and the PDR toward HD 200775 (Paper I). In this analysis, the three quantities  $n$ ,  $T$ , and  $I_{\text{UV}}$  are inferred from observed column densities of CH,  $\text{C}_2$ , and CN. However, only upper limits to the column densities are available for the  $\text{C}_2$  mol-

ecule toward HD 37903 and HD 147009 and for CN toward HD 147009, and as a consequence, the physical conditions in the foreground gas are not as well constrained as in other clouds (e.g., Paper I).

The rate equations used here are based on our earlier work. Federman & Huntress (1989) developed the chemistry for  $\text{C}_2$  in diffuse clouds, while Federman, Danks, & Lambert (1984) and Federman & Lambert (1988) did the same for CN. The incorporation of NH by Federman et al. (1994) into the rate equation for CN was the result of the

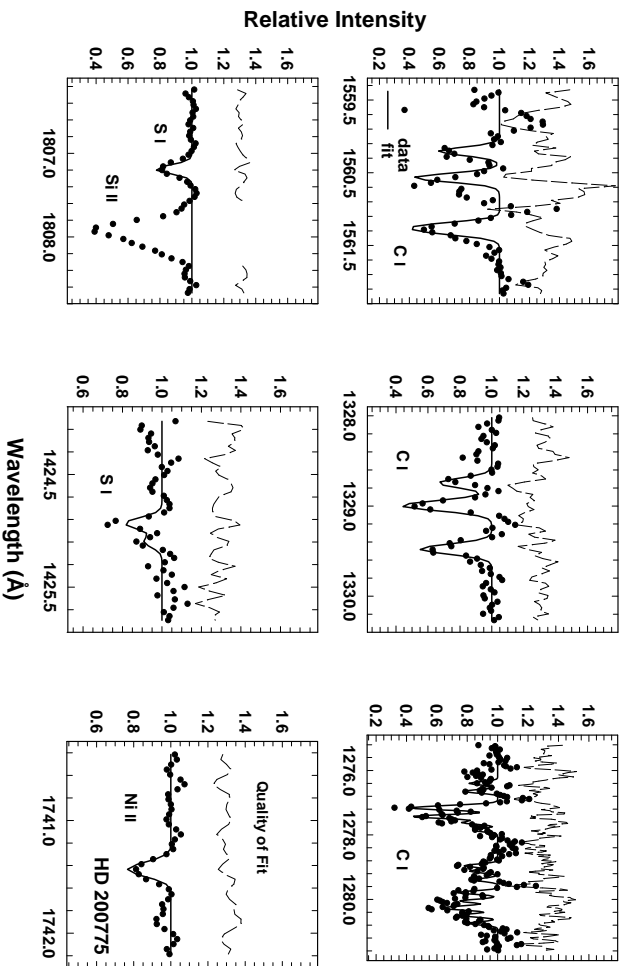


Fig. 8c

TABLE 7  
UV RESULTS FOR HD 37903 AND HD 200775

ABSORPTION FEATURE	WAVELENGTH (Å)	$f$	HD 37903		HD 200775		
			$W_{\lambda}(\text{obs})^a$ (mÅ)	$W_{\lambda}(\text{fit})$ (mÅ)	$W_{\lambda}^b$ (mÅ)	$W_{\lambda}(\text{obs})^a$ (mÅ)	$W_{\lambda}(\text{fit})$ (mÅ)
$^{12}\text{CO} (0-0)$ .....	1544.448	...	215 ± 15	...	191 ± 43	...	...
(1-0).....	1509.749	0.0291	43 ± 14	33	162 ± 15	186 ± 27	211
(2-0).....	1477.565	0.0401	27 ± 10	37	...	199 ± 37	203
(3-0).....	1447.352	0.0346	35 ± 10	34	26 ± 23	378 ± 57	234
(4-0).....	1419.044	0.0233	28 ± 8	27	24 ± 10	177 ± 15	176
(5-0).....	1392.525	0.0145	24 ± 9	19	58 ± 29	...	...
(6-0).....	1367.623	0.00795	...	...	...	170 ± 36	140
(7-0).....	1344.186	0.00414	...	...	...	109 ± 19	117
(8-0).....	1322.150	0.00200	...	...	...	113 ± 36	90
(9-0).....	1301.403	0.00095	...	...	...	82 ± 15	88
(10-0).....	1281.866	0.00041	...	...	...	81 ± 26	83
(11-0).....	1263.433	0.00018	...	...	...	67 ± 20	61
$^{13}\text{CO} (1-0)$ .....	1510.407	0.0351	...	...	...	266 ± 30	125
(2-0).....	1478.793	0.0402	...	...	...	133 ± 31	125
(3-0).....	1449.145	0.0347	...	...	...	125 ± 28	118
(4-0).....	1421.340	0.0242	...	...	...	112 ± 37	108
(5-0).....	1395.229	0.0145	...	...	...	117 ± 18	95
$\text{C I} (J=0)$ .....	1276.483	0.00168	...	3	41 ± 13	14 ± 10	24
( $J=1$ ).....	1280.135	0.0243	21 ± 6	20	...	90 ± 22	33
	1328.833	0.0580	34 ± 7	29	51 ± 11	27 ± 5	46
	1560.309	0.0804	34 ± 5	38	56 ± 14	64 ± 14	59
	1276.750	0.00239	15 ± 6	7	28 ± 9	22 ± 10	29
	1279.056	0.00202	11 ± 5	6	...	32 ± 11	29
	1279.890	0.0137	15 ± 4	18	...	52 ± 18	35
	1280.597	0.00684	14 ± 6	12	...	58 ± 21	33
	1329.085	0.0193	45 ± 5	54	70 ± 13	68 ± 7	124
	1560.682	0.0603	72 ± 7	60	67 ± 20	97 ± 12	110
( $J=2$ ).....	1277.723	0.0145	9 ± 4	7	30 ± 15	...	31
	1277.954	0.000967	5 ± 4	1	...	25 ± 15	21
	1279.229	0.00324	...	...	...	18 ± 8	24
	1279.498	0.000903	...	...	...	32 ± 11	21
	1280.847	0.00505	...	...	...	36 ± 15	25
	1329.578	0.0435	18 ± 5	21	41 ± 12	68 ± 9	76
	1561.340	0.0121	40 ± 8	34	...	126 ± 19	120

TABLE 7—Continued

ABSORPTION FEATURE	WAVELENGTH (Å)	$f$	HD 37903			HD 200775	
			$W_\lambda(\text{obs})^a$ (mÅ)	$W_\lambda(\text{fit})$ (mÅ)	$W_\lambda^b$ (mÅ)	$W_\lambda(\text{obs})^a$ (mÅ)	$W_\lambda(\text{fit})$ (mÅ)
Blends .....	1277.245	0.0967	70±7	62	78±11	113±16	131
	1277.513	0.0242	41±7	45	36±11	100±19	96
S I .....	1280.333	0.0147	18±5	15	...	77±16	60
	1295.653	0.087	10±3	9	15±7	8±4	22
	1316.543	0.0381	12±6	5	...	20±7	11
	1425.030	0.141	...	12	18±9	26±6	26
	1425.188	0.0269	...	...	...	14±6	11
	1472.971	0.0218	...	...	...	57±24	8
	1473.994	0.0803	...	8	30±15	10±5	21
	1474.379	0.0179	...	2	28±14	11±5	8
	1807.311	0.096	17±7	15	69±12	39±5	34
Ni II .....	1317.217	0.146	12±3	14	...	28±10	30
	1370.132	0.144	13±4	15	22±7	50±9	31
	1454.842	0.0516	9±4	8	...	28±9	27
	1709.600	0.0666	...	...	...	31±10	35
	1741.549	0.0776	15±5	15	36±8	41±7	37
	1751.910	0.0638	13±5	13	24±9	31±6	36

<sup>a</sup> IUE NEWSIPS data.

<sup>b</sup> Joseph et al. 1986.

discovery of NH in cloud envelopes (Meyer & Roth 1991). The respective equations for C<sub>2</sub> and CN are

$$N(\text{C}_2) = \frac{k_1 x(\text{C}^+) N(\text{CH}) n \alpha}{G(\text{C}_2) + k_2 x(\text{O}) n + k_3 x(\text{N}) n} \quad (1)$$

and

$$N(\text{CN}) = \frac{[k_3 x(\text{N}) N(\text{C}_2) + k_4 x(\text{N}) N(\text{CH}) + k_5 x(\text{C}^+) N(\text{NH}) \alpha] n}{G(\text{CN}) + k_6 x(\text{O}) n} \quad (2)$$

In these equations, the reaction rate constants are denoted by  $k_i$  (see Table 9); the abundance of species X relative to the proton abundance and the column density of species X are given by  $x(\text{X})$  and  $N(\text{X})$ , respectively. The total proton density [ $n(\text{H}) + 2n(\text{H}_2)$ ] is given by  $n$ , the photodestruction rate of species X is  $G(\text{X})$ , and  $\alpha$  accounts for the conversion of C<sup>+</sup> into CO (Federman et al. 1994). The rate constants for neutral-neutral reactions include a factor  $(T/300)^{0.5}$  to

TABLE 8

UV COLUMN DENSITIES FOR HD 37903 AND HD 200775

Species	HD 37903 $N(\text{fit})$ (cm <sup>-2</sup> )	HD 200775 $N(\text{fit})$ (cm <sup>-2</sup> )
$N_{\text{tot}}(^{12}\text{CO})$ .....	$(0.9\text{--}1.1) \times 10^{14}$	$(1.9\text{--}2.1) \times 10^{17}$
$N_{\text{tot}}(^{13}\text{CO})$ .....	...	$(1.0\text{--}1.2) \times 10^{16}$
$N_{\text{tot}}(\text{C I } (J=0))$ .....	$(1.1 \pm 0.5) \times 10^{14}$	$(3.2 \pm 1.0) \times 10^{16}$
$N_{\text{tot}}(\text{C I } (J=1))$ .....	$(1.5 \pm 0.5) \times 10^{14}$	$(3.6 \pm 1.3) \times 10^{16}$
$N_{\text{tot}}(\text{C I } (J=2))$ .....	$(3.5 \pm 1.2) \times 10^{13}$	$(3.2 \pm 1.5) \times 10^{16}$
$N_{\text{tot}}(\text{S I})$ .....	$(6.8 \pm 2.4) \times 10^{12}$	$(2.6 \pm 1.0) \times 10^{13}$
$N_{\text{tot}}(\text{Ni II})$ .....	$(1.1 \pm 0.6) \times 10^{13}$	$(1.0 \pm 0.3) \times 10^{14}$

account for the velocity term in the rate constant. The attenuation of radiation by dust is included in the photodissociation rate,  $G(\text{X}) = G_o I_{\text{UV}} \exp(-\tau_{\text{UV}})$ , where  $G_o$  is the rate at the surface of the cloud and  $\tau_{\text{UV}}$  is the optical depth at 1000 Å. A wavelength of 1000 Å for  $\tau_{\text{UV}}$  was chosen because it is in the middle of the range of wavelengths that leads to photodissociation of C<sub>2</sub> and CN ( $912 \leq \lambda \leq 1200$  Å) (Pouilly et al. 1983; Lavendy, Robbe, & Gandara 1987). The observed values of  $N(\text{CH})$  and  $N(\text{C}_2)$  were used in determining the predicted values of  $N(\text{C}_2)$  and  $N(\text{CN})$ . The value of  $N(\text{NH})$  was set to  $0.041N(\text{CH})$  since  $N(\text{NH})$  scales with  $N(\text{CH})$  (Meyer & Roth 1991; Federman et al. 1994).

The following considerations apply to the parameters  $\tau_{\text{UV}}$ ,  $\alpha$ , and  $x(\text{X})$ . From knowledge of the ratio of total to selective extinction,  $R_v = A_v/E(B-V)$ , and the ultraviolet

TABLE 9

RATES AND RATE CONSTANTS FOR THE CHEMICAL ANALYSIS

Reaction	Rate/Rate Constant	Value	Notes
$\text{C}^+ + \text{CH} \rightarrow \text{C}_2^+ + \text{H}$ .....	$k_1$	$3.0 \times 10^{-10} \text{ cm}^3 \text{ s}^{-1}$	a
$\text{C}_2 + \text{O} \rightarrow \text{CO} + \text{C}$ .....	$k_2$	$4.0 \times 10^{-11} \text{ cm}^3 \text{ s}^{-1}$	b, c
$\text{C}_2 + \text{N} \rightarrow \text{CN} + \text{C}$ .....	$k_3$	$1.7 \times 10^{-11} \text{ cm}^3 \text{ s}^{-1}$	c, d
$\text{CH} + \text{N} \rightarrow \text{CN} + \text{H}$ .....	$k_4$	$2.0 \times 10^{-11} \text{ cm}^3 \text{ s}^{-1}$	c, e
$\text{C}^+ + \text{NH} \rightarrow \text{all products}$ ...	$k_5$	$2.8 \times 10^{-10} \text{ cm}^3 \text{ s}^{-1}$	d
$\text{CN} + \text{O} \rightarrow \text{CO} + \text{N}$ .....	$k_6$	$1.8 \times 10^{-11} \text{ cm}^3 \text{ s}^{-1}$	e, f
$\text{C}_2 + h\nu \rightarrow 2\text{C}$ .....	$G_o(\text{C}_2)$	$2.0 \times 10^{-10} \text{ s}^{-1}$	g
$\text{CN} + h\nu \rightarrow \text{C} + \text{N}$ .....	$G_o(\text{CN})$	$1.0 \times 10^{-10} \text{ s}^{-1}$	h

<sup>a</sup> Federman & Huntress 1989.

<sup>b</sup> Estimate.

<sup>c</sup> Rate constant has a temperature dependence of  $(T/300)^{0.5}$ .

<sup>d</sup> Federman et al. 1994.

<sup>e</sup> Messing et al. 1981.

<sup>f</sup> Schmatjko & Wolfrum 1976.

<sup>g</sup> Pouilly et al. 1983, corrected for appropriate radiation field; van Dishoeck 1987.

<sup>h</sup> Lavendy et al. 1987.

extinction curve (CCM89; Buss et al. 1994), information on  $\tau_{UV}$  can be derived. For the direction toward HD 37903,  $\tau_{UV}$  was set at  $2A_v$ , with an  $R_v$  somewhat larger than average (Buss et al. 1994). Since the extinction curve for HD 147009 is similar to that seen for  $\rho$  Oph,  $\tau_{UV}$  toward  $\rho$  Oph (Federman et al. 1994) was scaled by  $E(B-V)$  to obtain the value for the sight line to HD 147009. For optical depths greater than 2, an additional term of the form  $\alpha = [1 + 14(\tau_{UV} - 2)/5]^{-1}$  (Federman et al. 1994) was added to account for the trends between the predicted and observed  $N(C_2)$  and  $\tau_{UV}$  caused by  $C^+$  being converted into CO (Federman & Huntress 1989). Fractional interstellar abundances of  $1.4 \times 10^{-4}$  (Sofia et al. 1997),  $7.5 \times 10^{-5}$  (Meyer, Cardelli, & Sofia 1997), and  $3.2 \times 10^{-4}$  (Meyer, Jura, & Cardelli 1998) for  $C^+$ , N, and O, respectively, were adopted from measurements with the *Hubble Space Telescope* (*HST*). These abundances account for modest depletion of the elements onto interstellar grains in cloud envelopes. These values are somewhat different than the fractional abundances quoted in Paper I: while the O and N abundances differ by 10%, the  $C^+$  abundance is almost a factor of 2 less. The lower fractional abundance of carbon requires a higher density for self-consistent chemical results, mainly because  $C_2$  is formed through reactions involving  $C^+$  and CH.

The column densities derived from the rate equations compare favorably with the observed columns for  $C_2$  and CN. The predicted column densities and inferred physical conditions are found in Table 10. The table also displays predictions for the molecular columns toward HD 200775 based on the atomic abundances adopted here; the greatest effect was on the extracted density. Changing the temperature did not significantly alter the predicted column densities in the chemical analysis above. The temperature used in this analysis was 40 K, the average value obtained from the C I excitation analysis ( $T \sim 50$  K) and the temperature determined from CO fractionation ( $T \sim 30$  K). The average of these two temperatures is reasonable in light of the fact that C I is more extended than CO in the cloud. The value of  $I_{UV}/n$  is the most important parameter in PDRs (HT99); it controls the chemistry and structure. When  $n$  was increased in our model,  $I_{UV}$  had to be increased in order to obtain the best match to the observed column densities. The ratio  $I_{UV}/n$  remained unchanged (see eqs. [1] and [2]).

### 3.2. Atomic Analysis

In this analysis, only the columns of Na I and K I associated with the molecular material (i.e., at the same velocity as the molecules CH, CN, and  $C_2$ ) are used. The atoms Na and K are predominantly singly ionized in interstellar space. Through ionization balance, we can analyze the neutral columns with the equation

$$N(X) = \frac{N_{\text{tot}}(H)A(X)\alpha(X)n_e\alpha_c}{G(X)}. \quad (3)$$

In this equation,  $A(X)$  is the elemental abundance;  $N_{\text{tot}}(H)$  is the total proton column density,  $N(H) + 2N(H_2)$ ;  $\alpha(X)$  is the radiative recombination rate constant (Péquignot & Aldrovandi 1986);  $G(X)$  is the photoionization rate for species X; and  $n_e$  is the electron density.  $A(X)$  includes depletion onto grains at about 25% for alkali elements (Phillips, Pettini, & Gondhalekar 1984), and  $\alpha_c$  incorporates the conversion of  $C^+$  into CO in the molecular material (as opposed to  $\alpha$  in the chemical analysis, which is an average for the total amount of neutral material). This conversion is a significant effect only when the fraction of molecular gas is  $\geq 50\%$  of the neutral gas. The form of  $\alpha_c$  is  $\alpha f + (1 - f)$ , where  $f$  is the  $H_2$  fraction  $[2N(H_2)/N_{\text{tot}}(H)]$  and  $\alpha$  is described in § 3.1. Many of the uncertain factors (e.g.,  $n_e$  and depletion) in the above equation can be eliminated by taking the ratio of  $N(\text{Na I})$  to  $N(\text{K I})$ . This ratio can be written as

$$\left[ \frac{N(\text{Na I})}{N(\text{K I})} \right] = \left[ \frac{A(\text{Na})}{A(\text{K})} \right] \left[ \frac{\alpha(\text{Na I})}{\alpha(\text{K I})} \right] \left[ \frac{G(\text{K I})}{G(\text{Na I})} \right]. \quad (4)$$

The appropriate value for  $A(\text{Na})/A(\text{K})$  is 16 and for  $\alpha(\text{Na I})/\alpha(\text{K I})$  is 1.05. The latter ratio was incorrectly given in Paper I; the change results in a 10% increase in the predicted ratio of Na I and K I columns. The predicted ratio mainly depends on the photoionization rates. The photoionization rates for Na I and K I at the cloud surface were determined from the measured ionization cross sections of Hudson & Carter (1967a) and of Hudson & Carter (1965, 1967b), Marr & Creek (1968), and Sandner et al. (1981), respectively.

To complete the atomic analysis, details about the extinction curve are needed. The main difference for the two sight lines studied here involves the effect of extinction from interstellar grains. The pair method (WBS84) was used to derive

TABLE 10  
RESULTS OF THE CHEMICAL ANALYSIS

Physical Parameters	HD 37903	HD 147009	HD 200775
$n$ ( $\text{cm}^{-3}$ )	500–1500	400–1200	300–900
$T$ (K)	40	40	40
$I_{UV}$	1.0–3.0	1.0–3.0	1.0–3.0
$E(B-V)$	0.35 <sup>a</sup>	0.38 <sup>a</sup>	0.45 <sup>a</sup>
$\tau_{UV}$	2.9 <sup>b</sup>	1.7 <sup>c</sup>	4.05 <sup>d</sup>
$N(\text{CH})_{\text{obs}}$ ( $\text{cm}^{-2}$ )	$(9.2 \pm 0.1) \times 10^{12}$	$(1.5 \pm 0.1) \times 10^{13}$	$(3.2 \pm 0.2) \times 10^{13d}$
$N(C_2)_{\text{obs}}$ ( $\text{cm}^{-2}$ )	$\leq 9.9 \times 10^{12}$	$\leq 3.4 \times 10^{13}$	$1.2 \times 10^{13d}$
$N(C_2)_{\text{pred}}$ ( $\text{cm}^{-2}$ )	$4.0 \times 10^{12}$	$6.5 \times 10^{12}$	$1.2 \times 10^{13}$
$N(\text{CN})_{\text{obs}}$ ( $\text{cm}^{-2}$ )	$(7.9 \pm 1.5) \times 10^{11}$	$\leq 8.3 \times 10^{11}$	$(1.2 \pm 0.3) \times 10^{13d}$
$N(\text{CN})_{\text{pred}}$ ( $\text{cm}^{-2}$ )	$8.5 \times 10^{11}$	$7.4 \times 10^{11}$	$3.9 \times 10^{12}$

<sup>a</sup> For HD 37903 and HD 200775 (Buss et al. 1994) and for HD 147009 (Racine 1968).

<sup>b</sup>  $\tau_{UV} = 2A_v$ , but  $R_v = 4.11$  (Buss et al. 1994), somewhat larger than average.

<sup>c</sup> Extinction is similar to the value toward  $\rho$  Oph,  $\tau_{UV}$  scaled by  $E(B-V)$ .

<sup>d</sup> Paper I.

the extinction curve for the central star in the nebula vdB 102, HD 147009. Extinction curves for two other stars, HD 37023 and HD 37903, were computed for comparison with extinction curves derived by Fitzpatrick & Massa (1990, hereafter FM90). Stellar spectra of HD 31726, HD 37023, HD 37903, HD 55857, HD 64802, HD 147009, and  $\zeta$  Aql were obtained from the *IUE* archive; the file names are listed in Table 6. The unreddened standard stars used in FM90 are used in this work, with the exception of  $\zeta$  Aql (Witt, Bohlin, & Stecher 1981), in order to obtain the most consistent results. The extinction curves for HD 37023 and HD 37903 derived by FM90 are similar to those derived by us, demonstrating that the extinction curve for HD 147009 derived here is reliable.

The extinction curves for HD 37903 and HD 147009 were found to be anomalous when compared to the one representing typical Galactic extinction, that for  $\zeta$  Per (Savage & Mathis 1979). For this analysis, the extinction curve for  $\zeta$  Per was scaled to the same reddening parameter of the observed star. Figure 9 displays the resulting extinction curves. Since the photoionization rates were determined for  $\zeta$  Per (Paper I), the difference between extinction toward the reddened line of sight compared to the average is used to derive an attenuated photoionization rate for the reddened star. Changes in extinction introduce a multiplicative factor to the photoionization rates of the form  $10^\beta$ . For the wavelengths where the curve for  $\zeta$  Per shows more (less) extinction, the exponent  $\beta$  is positive (negative). Since the two extinction curves can intersect, the extinction can be enhanced for some wavelength intervals and diminished for others. The total rate is the sum of the rates for each wavelength interval.

### 3.3. Atomic Results

The atomic spectra for Ca II H and K and Na I D exhibit six velocity components along the line of sight toward HD 37903 (see Fig. 1). There is no molecular absorption seen in five of them. The atomic gas not associated with molecular absorption is attributed to Orion's cloak. Orion's cloak is a rapidly ( $35 \leq v \leq 120 \text{ km s}^{-1}$ ) expanding shell of gas centered on the Orion OB1 association (Cowie, Songaila, & York 1979). While the five velocity components toward HD 37903 have lower velocities ( $\leq 30 \text{ km s}^{-1}$ ) than is seen in Orion's cloak, this velocity structure is observed toward many other stars in Orion (Cowie et al. 1979; Welty et al. 1994, 1996) showing the high-velocity gas of Orion's cloak. Our atomic analysis involves only absorption associated with the molecular material in the nebula.

The atomic observations yield information on the photoionization rates present in the gas (see eq. [4]) because equation (4) is not dependent on the physical conditions. Toward  $\zeta$  Per, an observed ratio Na I/K I of  $100 \pm 6$  was obtained. For the predicted ratio a refined analysis was performed. The difference in grain attenuation between 2400 and 2900 Å ( $\Delta A_\lambda = 0.2$ ) was taken into account. This resulted in a predicted ratio of 67. Toward HD 200775, the observed ratio is  $54 \pm 9$ , which is in excellent agreement with the predicted ratio of 54 when the effects of the extinction curve are applied. (Note that the sum of all velocity components of Na I and K I is used for this sight line; see § 4.4.)

The observed column densities were  $(1.1 \pm 0.2) \times 10^{13}$  and  $1.1 \times 10^{11} \text{ cm}^{-2}$  for Na I and K I toward HD 37903, giving an observed ratio of  $100 \pm 18$ . The inferred Na I and

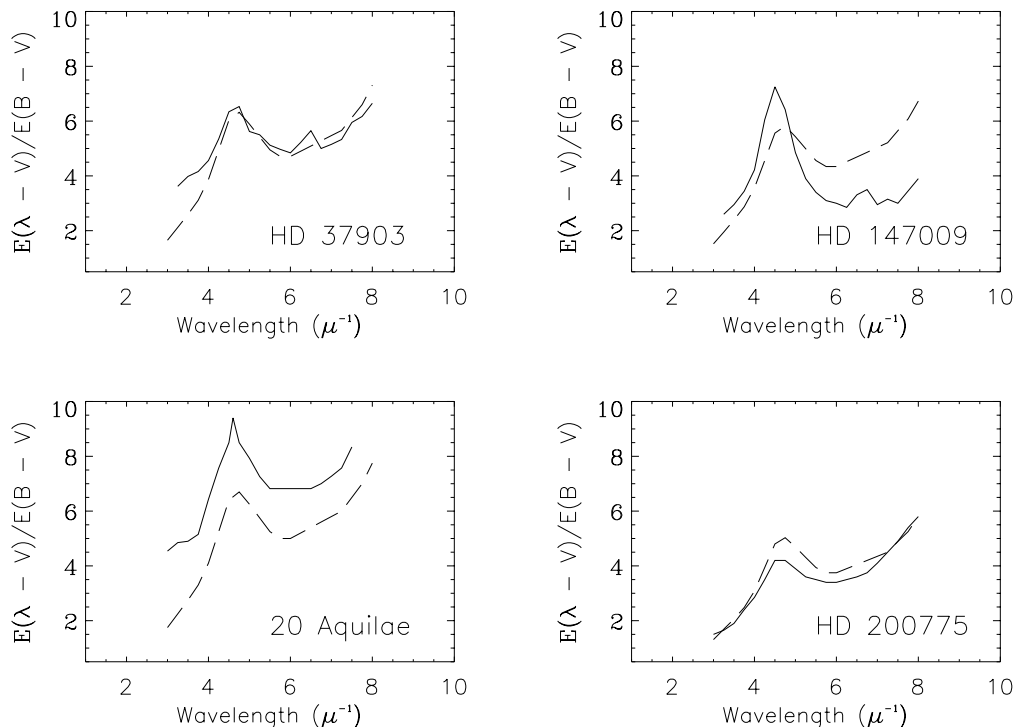


FIG. 9.—Derived extinction curves for the reddened lines of sight. The dashed curve is the average interstellar extinction curve represented by  $\zeta$  Per scaled to the  $E(B - V)$  of the reddened star. Extinction curves for  $\zeta$  Per, 20 Aql, and HD 200775 were obtained from Savage & Mathis (1979), Savage et al. (1985), and Walker et al. (1980), respectively.

K I photoionization rates are  $1.2 \times 10^{-11}$  and  $4.4 \times 10^{-11}$   $s^{-1}$ , which yield a predicted ratio of 62. For the line of sight to HD 147009, the observed column densities of  $(1.5 \pm 0.3) \times 10^{13}$  and  $(2.3 \pm 0.1) \times 10^{11}$   $cm^{-2}$  for Na I and K I, respectively, were determined. These columns produce an observed ratio of  $65 \pm 13$ . The Na I and K I photoionization rates for this gas are  $2.9 \times 10^{-10}$  and  $9.7 \times 10^{-10}$   $s^{-1}$ , respectively. These values lead to a predicted ratio of 56. As expected, the correspondence between observed and predicted  $N(\text{Na I})/N(\text{K I})$  ratios is good.

Another useful way to study the observed atomic abundances is to compare, for a specific atom, the column density obtained toward the program stars to the column density obtained toward  $\zeta$  Per. In this way we check for potential differences in depletion onto grains and  $n_e$  (see eq. [3]). Curves of growth with  $b = 1.5$   $km\ s^{-1}$  for the weak Na I doublet at 3302 Å (Crutcher 1975) as well as the strong D lines at 5889 and 5895 Å (Hobbs 1974a, 1974b; Welty et al. 1994; B.-G. Andersson 2000, private communication) and the weak K I doublet at 4044 and 4047 Å (Knauth et al. 2000) yielded weighted average column densities for Na I of  $(7.3 \pm 0.3) \times 10^{13}$  and  $(7.3 \pm 0.3) \times 10^{11}$   $cm^{-2}$  for K I toward  $\zeta$  Per. Our precise column density measurements of K I  $\lambda\lambda 4044, 4047$  yield similar results to the column density obtained from the K I  $\lambda 7699$  line. The photoionization rates of Na I and K I toward  $\zeta$  Per are  $4.5 \times 10^{-12}$  and  $1.8 \times 10^{-11}$   $s^{-1}$  (Paper I). For this analysis we require the total proton density toward each star. The proton density is  $(1.6 \pm 0.3) \times 10^{21}$   $cm^{-2}$  toward  $\zeta$  Per (Bohlin, Savage, & Drake 1978) and  $(3.6 \pm 0.7) \times 10^{21}$   $cm^{-2}$  toward HD 37903 (Buss et al. 1994). Toward HD 147009, the total proton column density was determined from several sources. From radio observations of CH, the column density of  $H_2$  was found to be  $2.5 \times 10^{20}$   $cm^{-2}$  (Vallée 1987) using the relationship derived by Federman (1982) and Danks, Federman, & Lambert (1984). A value of  $N(H\ I) = 1.1 \times 10^{21}$   $cm^{-2}$  was determined from the 21 cm results of Cappa de Nicolau & Pöppel (1986), indicating  $N_{\text{tot}}(H) = 1.6 \times 10^{21}$   $cm^{-2}$ . Also from 21 cm observations, de Geus & Burton (1991) derived  $N(H\ I) = 1.8 \times 10^{21}$   $cm^{-2}$ , which yields  $N_{\text{tot}}(H) = 2.3 \times 10^{21}$   $cm^{-2}$ . The average

proton column density toward HD 147009 is therefore  $(1.9 \pm 0.4) \times 10^{21}$   $cm^{-2}$ . In our analysis, we adopted a 20% error in  $N_{\text{tot}}(H)$  for all stars except HD 200775 where the observed precision was higher.

Most of the total proton density is assumed to lie in front of HD 147009, since most of  $N(H\ I)$  resides in one component (Cappa de Nicolau & Pöppel 1986) and the star is at high Galactic latitude,  $b = 20^\circ 894$  (ddL89). The relationship of Bohlin et al. (1978),  $N_{\text{tot}}(H)/E(B-V) = 5.8 \times 10^{21}$  atoms  $cm^{-2}$   $mag^{-1}$ , supports this assumption. This relationship yields  $N_{\text{tot}}(H) = 2.2 \times 10^{21}$   $cm^{-2}$ , which is similar to the column density determined above. Therefore, it is reasonable to assume that all of the neutral hydrogen resides in front of the star.

Estimates for gas density, temperature, and UV field strength are needed to complete this analysis. The values of  $n$ ,  $T$ , and  $I_{UV}$  toward  $\zeta$  Per (Federman et al. 1994) were rederived with the new values for the fractional abundances of  $C^+$ , N, and O, resulting in 1200  $cm^{-3}$ , 40 K, and 1. For the gas toward HD 37903 and HD 147009, the adopted values of  $n$  and  $T$  are from the chemical analysis above for  $I_{UV} = 1$  (see Table 10). Here we set  $n_e = nX(C^+)$ , since the electrons mostly come from ionized carbon. The predicted ratios toward HD 200775 are  $0.05 \pm 0.01$  and  $0.06 \pm 0.01$  for Na I and K I, respectively. The observed ratios are  $0.08 \pm 0.01$  and  $0.15 \pm 0.02$  for Na I and K I, respectively. (These ratios are based on our refined analysis and differ somewhat from the ratios in Paper I.) For the case of HD 37903, the effect of  $\alpha_c$  needed to be included since the fraction of molecular gas is  $\geq 50\%$ . This resulted in a predicted ratio  $N(\text{Na I})_{\text{HD 37903}}/N(\text{Na I})_{\zeta\text{ Per}}$  of  $0.23 \pm 0.06$  and  $0.21 \pm 0.06$  for K I. The observed ratios are  $0.15 \pm 0.03$  for Na I and  $0.15 \pm 0.01$  for K I. As for the PDR toward HD 147009, the analysis gives a ratio of  $0.01 \pm 0.01$  for both ratios. The observed column density ratios are  $0.21 \pm 0.04$  for Na I and  $0.32 \pm 0.02$  for K I.

The results of our analysis are summarized in Table 11. It can be seen from the ratios of Na I and especially K I that a modest change in  $n_e$  and/or depletion onto grains is needed to bring the predictions and observations for the foreground PDR of NGC 7023 into agreement. This change

TABLE 11  
RESULTS OF THE ATOMIC ANALYSIS

Physical Parameters	$\zeta$ Per	HD 37903	HD 147009	HD 200775
$n$ ( $cm^{-3}$ )	1200 <sup>a</sup>	500 <sup>a</sup>	400 <sup>a</sup>	300 <sup>a</sup>
$G_o(\text{Na I})$ $s^{-1}$	$4.5 \times 10^{-12}$	$1.2 \times 10^{-11}$	$2.9 \times 10^{-10}$	$3.4 \times 10^{-11b}$
$G_o(\text{K I})$ $s^{-1}$	$1.8 \times 10^{-11}$	$4.4 \times 10^{-11}$	$9.7 \times 10^{-10}$	$1.1 \times 10^{-10b}$
$N(\text{Na I})_{\text{obs}}$ ( $cm^{-2}$ )	$(7.3 \pm 0.3) \times 10^{13c}$	$(1.1 \pm 0.2) \times 10^{13c}$	$(1.5 \pm 0.3) \times 10^{13c}$	$(5.9 \pm 0.8) \times 10^{12b}$
$N(\text{K I})_{\text{obs}}$ ( $cm^{-2}$ )	$(7.3 \pm 0.3) \times 10^{11c}$	$1.1 \times 10^{11}$	$(2.3 \pm 0.1) \times 10^{11c}$	$(1.1 \pm 0.1) \times 10^{10b}$
$N_{\text{tot}}(H)$ ( $cm^{-2}$ )	$(1.6 \pm 0.3) \times 10^{21d}$	$(3.6 \pm 0.7) \times 10^{21d}$	$(1.9 \pm 0.4) \times 10^{21d}$	$(2.3 \pm 0.3) \times 10^{21b}$
$(\text{Na I}/\text{K I})_{\text{pred}}$	67 <sup>e</sup>	62	56	54 <sup>e</sup>
$(\text{Na I}/\text{K I})_{\text{obs}}$	$100 \pm 6$	$100 \pm 18$	$65 \pm 13$	$54 \pm 9^b$
$(\text{Na I}_{\text{star}}/\text{Na I}_{\zeta\text{ Per}})_{\text{pred}}$	...	$0.23 \pm 0.06$	$0.01 \pm 0.01$	$0.05 \pm 0.01^e$
$(\text{Na I}_{\text{star}}/\text{Na I}_{\zeta\text{ Per}})_{\text{obs}}$	...	$0.15 \pm 0.03$	$0.21 \pm 0.04$	$0.08 \pm 0.01^e$
$(\text{K I}_{\text{star}}/\text{K I}_{\zeta\text{ Per}})_{\text{pred}}$	...	$0.21 \pm 0.06$	$0.01 \pm 0.01$	$0.06 \pm 0.01^e$
$(\text{K I}_{\text{star}}/\text{K I}_{\zeta\text{ Per}})_{\text{obs}}$	...	$0.15 \pm 0.01$	$0.32 \pm 0.02$	$0.15 \pm 0.02^e$

<sup>a</sup> For  $I_{UV} = 1.0$ .

<sup>b</sup> Paper I.

<sup>c</sup>  $b = 1.5$   $km\ s^{-1}$  for  $\zeta$  Per and HD 147009 and  $2.0$   $km\ s^{-1}$  for HD 37903.

<sup>d</sup> Assumes a 20% error in  $N_{\text{tot}}(H)$ .

<sup>e</sup> Includes improvements and corrections to Paper I; see text for details.

from Paper I is caused by the decrease in  $x(\text{C}^+)$ . Since the observed and predicted results for Na I and K I toward HD 37903 with respect to  $\zeta$  Per agree within the errors, our estimates for  $n_e$  and depletion for the foreground material toward HD 37903 are reasonable. The situation is more extreme for the foreground PDR of vdB 102. A factor of 20 increase in  $n_e$  is needed to bring the predictions into agreement with the observations. While the flat FUV extinction curve for HD 147009 allows more radiation to permeate the nebula,  $n_e$  is limited by the elemental abundance of carbon. Because HD 147009 is an A0 V star, enhanced ionization in an H II region is not expected, unless the enhanced ionization arises from the combined effects of other, earlier type stars in Sco OB2.

#### 3.4. UV Results

The IUE data on C I and CO provide additional constraints on the physical conditions for the foreground PDR. The relative populations of fine-structure levels in the electronic ground state of C I arise from a combination of collisional excitation and de-excitation, radiative decay, and enhanced radiation fields, UV pumping. Analysis of the observed distribution via statistical equilibrium yields pressure ( $n_{\text{tot}}T$ ) and sometimes  $I_{\text{UV}}$ . Here  $n_{\text{tot}}$  is the density of collision partners,  $n(\text{H}) + n(\text{H}_2)$ . If the kinetic temperature is known from another diagnostic,  $n_{\text{tot}}$  can be obtained and compared with  $n [n(\text{H}) + 2n(\text{H}_2)]$  inferred from the chemistry. The ratio of  $N(^{12}\text{CO})/N(^{13}\text{CO})$  is affected by chemical fractionation. When the gas is cold ( $T \leq 40$  K) and is permeated by a strong UV radiation field so that the abundance of  $\text{C}^+$  is high, the ratio of columns is less than the ratio of ambient  $^{12}\text{C}/^{13}\text{C}$  (about 60) because  $^{13}\text{CO}$  has the lower zero-point energy (see Watson, Anicich, & Huntress 1976). If the gas is not especially cold but is still affected by UV photons, selective isotopic photodissociation enhances  $N(^{12}\text{CO})$  relative to  $N(^{13}\text{CO})$  (e.g., Bally & Langer 1982; van Dishoeck & Black 1988). The enhancement is the result of  $^{12}\text{CO}$  self-shielding itself from photodissociation because its lines are more optically thick.

The analysis of C I excitation described by Lambert et al. (1994) forms the basis of our results. In particular, their collisional rate constants and radiative rates are adopted here. The fractional abundances of collisional partners are based on the observations of Buss et al. (1994; see also Table 12, with the added assumption that 10% of the gas is He). The analysis also assumes that absorption from each fine-structure level,  $J$ , arises from the same parcel of gas. Figure 10 shows the results of our calculations. Here we plot the density and temperature consistent with the observed column density ratios,  $N(J=1)/N(J=0)$  (dashed curves) and  $N(J=2)/N(J=0)$  (dot-dashed curves). The upper and lower bounds are based on  $\pm 1 \sigma$  errors in column density. For HD 37903, results for  $I_{\text{UV}}$  of 3 are indistinguishable from those with  $I_{\text{UV}}$  of 1. The strongest constraint comes from  $N(2)/N(0)$ :  $n_{\text{tot}}$  lies between 300 and  $500 \text{ cm}^{-3}$  for  $T$  about 50 K. Based on the observed columns of H and  $\text{H}_2$ , the inferred value for  $n$  is  $400\text{--}700 \text{ cm}^{-3}$ . As for the foreground PDR toward HD 200775, the lower limits from  $N(2)/N(0)$  and the upper limits from  $N(1)/N(0)$  indicate that  $n_{\text{tot}}$  is about  $700 \text{ cm}^{-3}$  (or  $n$  is  $\approx 850 \text{ cm}^{-3}$ ) for  $T$  between 40 and 60 K. Analysis of  $\text{C}_2$  excitation from the data in Paper I is consistent with the C I results if  $I_{\text{IR}}$  is 3. For  $\text{C}_2$ , optical pumping to an excited electronic state

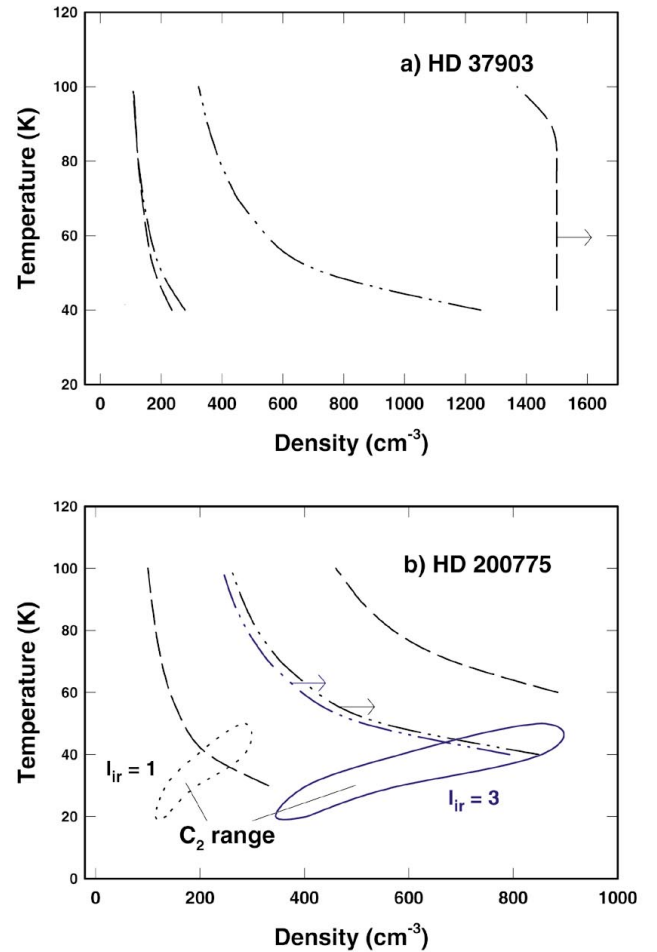


FIG. 10.—Results of C I excitation for HD 37903 and HD 200775. Density is for collisional partners (see text). The  $N(J=1)/N(J=0)$  ratio (dashed lines) and the  $N(J=2)/N(J=0)$  ratio (dot-dashed lines) based on  $\pm 1 \sigma$  uncertainty in column densities are shown. (a) For HD 37903, the arrow indicates that the upper range for the  $N(J=1)/N(J=0)$  ratio is a lower limit. Results for  $I_{\text{UV}} = 3$  are indistinguishable for  $I_{\text{UV}} = 1$ . (b) For HD 200775, the upper limit for the  $N(J=2)/N(J=0)$  ratio yields much larger density. Blue scale shows results for threefold enhancement in radiation field where distinguishable. The result from  $\text{C}_2$  excitation is also shown.

involves absorption of infrared radiation, hence the use of  $I_{\text{IR}}$ . [Again, the curves for  $I_{\text{UV}}$  of 3 are essentially those for  $I_{\text{UV}}$  of 1, except for the lower range allowed by  $N(2)/N(0)$ .]

The inferred values for  $n$  agree with the chemical results for the two foreground PDRs. The gas containing C I toward HD 37903 appears to have a density most consistent with the chemical results for  $I_{\text{UV}} = 1$ . Since C I may occupy a larger volume of material than the molecules  $\text{C}_2$  and CN, the inferred average density from C I excitation could be smaller by about a factor of 2 compared to the density in CN-rich gas. This seems to be the case for  $\zeta$  Oph (Lambert et al. 1994). In other words, the chemical results for  $I_{\text{UV}}$  of 1–3 are still consistent with the results from C I. The situation is different for the gas toward HD 200775. Here the C I results are most consistent with the chemical results for  $I_{\text{UV}}$  of 3. Since this comparison also applies to the results for  $\text{C}_2$  with  $I_{\text{IR}}$  of 3, the strengths of the UV and IR fields seem to scale together for the foreground PDR.

The observations of HD 200775 reveal that  $N(^{12}\text{CO})/ N(^{13}\text{CO})$  is about 20. An enhancement in  $N(^{13}\text{CO})$  arises when the gas is cold, yet it contains an appreciable fraction of  $\text{C}^+$ . Lambert et al. (1994) described the amount of fractionation in terms of the quantity  $F_{13}$ , the column density ratio divided by the ambient  $^{12}\text{C}/^{13}\text{C}$  ratio. When the ratio of columns is smaller than the ambient ratio,  $F_{13}$  equals  $\exp(-35/T)$ . Since the gas toward HD 200775 has  $F_{13}$  of  $\approx 0.33$ , the CO observations indicate a temperature of 30–35 K. The need for  $\text{C}^+$  suggests that the UV radiation field is somewhat higher than in a typical diffuse cloud, consistent with the results described above. Since  $^{13}\text{CO}$  was not detected toward HD 37903, no meaningful analysis is possible.

#### 4. DISCUSSION

##### 4.1. Structure of PDRs

Since  $I_{\text{UV}}/n$  determines the structure of PDRs (HT99), we can estimate the fraction of foreground material in the PDR. We use equation (7) from Hollenbach & Tielens (1999), which approximately relates the formation rate of  $\text{H}_2$  to the photodissociation rate, for  $N_{\text{tot}}(\text{H}) \leq 10^{21} \text{ cm}^{-2}$ . As a result of its approximate nature, we assume that the use of this equation for lines of sight with  $N_{\text{tot}}(\text{H})$  of a few times  $10^{21} \text{ cm}^{-2}$  is valid as well. This steady state expression is used to reproduce the column of  $\text{H}_2$ , assuming that the observed  $\text{H}_2$  is completely within the PDR:

$$N(\text{H}_2) = \frac{[N_{\text{tot}}(\text{H})A]^4 N_o}{N_o^4} = \frac{[nN_{\text{tot}}(\text{H})\gamma_{\text{H}_2}]^4 N_o}{[4I_{\text{diss}}(0)N_o]^4}. \quad (5)$$

In this equation,  $N_o$  is the column density at which self-shielding becomes important ( $N_o = 1 \times 10^{14} \text{ cm}^{-2}$ ),  $\gamma_{\text{H}_2}$  is the formation rate of  $\text{H}_2$  on grains ( $\gamma_{\text{H}_2} = 3 \times 10^{-17} \text{ cm}^3 \text{ s}^{-1}$ ), and  $I_{\text{diss}}(0)$  is the photodissociation rate ( $4 \times 10^{-11} I_{\text{UV}} \text{ s}^{-1}$ ). Table 12 shows that the predicted values for  $I_{\text{UV}}$  are 30–60 times greater than the values derived from the chemical analysis. The  $I_{\text{UV}}$  determined from the chemistry must be the same as that determined from the above equation for  $\text{H}_2$ ; these results suggest that only a small fraction ( $\sim 3\%$ ) of the foreground material is actually associated with the PDR in front of the star.

The linear extent of the foreground PDR ( $L_{\text{tr}}$ ) can be compared to that in the background molecular cloud. We adopted the expression for  $L_{\text{tr}}$  of Federman, Glassgold, & Kwan (1979):

$$L_{\text{tr}} = \frac{2.93 \times 10^{14} n^{-2.4} (5.6 \times 10^{-11} I_{\text{UV}})^{1.4}}{(2\gamma_{\text{H}_2})^{1.4}} \text{ cm}. \quad (6)$$

TABLE 12  
INDEPENDENT DETERMINATION OF  $I_{\text{UV}}/n$

Parameters	HD 37903	HD 147009	HD 200775
$(I_{\text{UV}}/n) \text{ (cm}^3\text{)} \dots\dots\dots$	$2.0 \times 10^{-3a}$	$2.5 \times 10^{-3a}$	$3.3 \times 10^{-3b}$
$N_{\text{tot}}(\text{H})_{\text{obs}} \text{ (cm}^{-2}\text{)} \dots\dots\dots$	$3.6 \times 10^{21c}$	$1.9 \times 10^{21d}$	$2.3 \times 10^{21b}$
$N(\text{H}_2)_{\text{obs}} \text{ (cm}^{-2}\text{)} \dots\dots\dots$	$1.0 \times 10^{21e}$	$2.5 \times 10^{20e}$	$3.2 \times 10^{20e}$
$(I_{\text{UV}}/n)_{\text{H}_2} \text{ (cm}^3\text{)} \dots\dots\dots$	0.12	0.09	0.10

<sup>a</sup> From Table 10.

<sup>b</sup> Federman et al. 1997, with corrections; see text for details.

<sup>c</sup> Buss et al. 1994.

<sup>d</sup> From Table 11.

<sup>e</sup> Vallée 1987.

For the foreground PDR of NGC 2023, this equation yields an extent of 0.002–0.007 pc for densities of 500–1500  $\text{cm}^{-3}$  and respective values for  $I_{\text{UV}}$  of 1–3. For the background cloud with  $n$  of  $10^5 \text{ cm}^{-3}$  and  $I_{\text{UV}}$  of  $10^4$  (Rouan et al. 1997), the extent is 0.0086 pc. For NGC 7023, the range in extent is 0.008–0.03 pc when  $n$  of 300–900  $\text{cm}^{-3}$  and  $I_{\text{UV}}$  of 1–3, respectively, are used for the foreground cloud. Utilizing the density ( $10^4 \text{ cm}^{-3}$ ) and  $I_{\text{UV}}$  of  $10^3$  from Rogers, Heyer, & Dewdney (1995) for the background cloud indicates a length scale of 0.086 pc. The extent of the PDR into the molecular cloud behind the stars is comparable to its extent in the lower density foreground gas. For vdB 102, information is only available for the foreground gas; an extent of 0.004–0.01 pc is found from densities and  $I_{\text{UV}}$  of 400–1200  $\text{cm}^{-3}$  and 1–3, respectively.

From the column of neutral hydrogen and the density of the cloud, one can estimate the size of the neutral cloud in front of the star, assuming that all the hydrogen is associated with the cloud. Toward HD 37903, a neutral cloud size of 0.8–2.3 pc is derived. Cloud sizes of 0.5–1.5 pc toward HD 147009 and 0.8–2.5 pc toward HD 200775 are obtained. These simple calculations show that the PDR does indeed reside in a small fraction ( $\sim 1\%$ ) of the neutral cloud.

##### 4.2. NGC 2023

In order to arrive at a consistent model of PDRs associated with these reflection nebulae, it is necessary to compare the results obtained here to the physical conditions inferred from diagnostics at other wavelengths of the background molecular cloud. As noted in § 1.1, there have been many studies of NGC 2023 whose focus was the molecular cloud behind HD 37903. Here we highlight those studies that relate to our measurements.

Infrared  $\text{H}_2$  observations (Martini et al. 1999 and references therein) of this nebula show that there is a neutral shell of molecular material 0.13–0.20 pc from the star. However, this neutral shell is not seen in the H I data. The H I emission is observed to be centered on HD 37903 (Lebrón & Rodríguez 1997). Clumps of material have been detected in the nebula on less than parsec size scales (Martini et al. 1999). This implies that there are two components within the nebula. Steiman-Cameron et al. (1997) determined that the densities for the low- and high-density components are 750 and  $10^5 \text{ cm}^{-3}$ , respectively, with a temperature range of  $250 \leq T \leq 750 \text{ K}$  and a radiation field of  $1.5 \times 10^4$  times the average interstellar radiation field. For the gas directly behind HD 37903, Wyrowski et al. (1997) found a density of  $3 \times 10^4 \text{ cm}^{-3}$ , a radiation field  $\sim 500$  times the average interstellar radiation field (ISRF), and a temperature of 125 K.

Martini et al. (1999) measured the near-infrared emission from  $\text{H}_2$  in two regions, 60" south and 160" north of HD 37903. Their results show that these regions are of relatively high density,  $n \sim 10^5\text{--}10^6 \text{ cm}^{-3}$ , with a ratio of radiation field to density  $I_{\text{UV}}/n \sim 0.1\text{--}0.01 \text{ cm}^3$ . These measurements are in agreement with other studies that find high-density clumps ( $10^5\text{--}10^7 \text{ cm}^{-3}$ ) in a slightly less dense interclump medium ( $\sim 10^4\text{--}10^5 \text{ cm}^{-3}$ ) with an enhancement of the UV radiation field over the average ISRF of  $10^3\text{--}10^4$  for NGC 2023 (Martini et al. 1999; Takami et al. 2000).

Our chemical analysis reveals that the radiation field is weaker in the foreground material,  $I_{\text{UV}} \sim 1\text{--}3$ , than the values determined in previous work for the molecular cloud behind the star (Field et al. 1994, 1998; Fuente et al. 1995;



Steiman-Cameron et al. 1997; Wyrowski et al. 1997). The density of the foreground gas has a range of a few times  $10^2$ – $10^3$   $\text{cm}^{-3}$ , a factor of 10–1000 less dense than the gas in the molecular cloud behind HD 37903. The temperature of the foreground gas is a factor of 2 less than the material behind the star. These observations of the foreground material indicating lower densities support the idea that HD 37903 formed near the edge of the molecular cloud and rapidly dispersed the material at the edge of the cloud. NGC 2023 could be a face-on example of star formation by the blister model (Zuckerman 1973; Israel 1978).

Burton et al. (1998) indicate clump densities of  $\approx 10^4$   $\text{cm}^{-3}$  and an FUV radiation field about  $10^3$  times the ambient interstellar value at a projected distance of 0.18 pc. Buss et al. (1994) measured a stellar flux at 1050 Å of  $1.5 \times 10^{-11}$   $\text{ergs cm}^{-2} \text{s}^{-1} \text{Å}^{-1}$ . Using an average interstellar flux of  $2.65 \times 10^{-6}$   $\text{ergs cm}^{-2} \text{s}^{-1} \text{Å}^{-1}$ ,  $\tau_{\text{UV}} = 2.9$ , and a distance to the star of 470 pc (Perryman et al. 1997), we find a distance to the foreground gas of 2.5–4.5 pc for our values of  $I_{\text{UV}}$  between 1 and 3. Therefore, the radiation field at a distance of 0.1–0.2 pc from the star would be 500–2000 times the average radiation field, which is consistent with the Burton et al. (1998) value of  $I_{\text{UV}} \sim 1000$  (usually denoted by  $G_0$ ) at a distance 0.18 pc from the star.

From maps of CN  $J = 1 \rightarrow 0$  (113.5 GHz) and HCN  $J = 1 \rightarrow 0$  (88.6 GHz) emission, Fuente et al. (1995) detected an enhanced amount of CN in the molecular shell in NGC 2023. The CN/HCN ratio inside the  $\text{H}_2$  shell was found to be 25 times larger than outside. Outside the shell this ratio is close to the interstellar value for molecular clouds ( $\approx 2$ ). HCN photodissociation plays an important role because it produces CN and because the photodissociation rate of HCN is greater than that of CN. While we previously found an enhancement in the abundance of CN toward HD 200775 (Paper I), consistent with radio observations of NGC 7023 (Fuente et al. 1993), our chemical results for the foreground PDR of NGC 2023 show no such enhancement. Most of the CN is in the envelope of the molecular cloud, not in the foreground PDR.

#### 4.3. *vdB 102*

The chemical analysis for HD 147009 matches well with the observed upper limits for  $\text{C}_2$  and CN, but the physical conditions derived in our chemical analysis could not be constrained well. Unfortunately, little is known about the physical conditions in this nebula. Kutner et al. (1980) mapped CO emission in reflection nebulae and determined that the peak CO emission is offset, about 3/3 to the northeast, from the star. From radio observations of CH in the cloud, a column density  $N(\text{CH}) = (1.0 \pm 0.3) \times 10^{13}$   $\text{cm}^{-2}$  was obtained (Vallée 1987). This is comparable to the column density obtained from our measurements,  $N(\text{CH}) = (1.5 \pm 0.1) \times 10^{13}$   $\text{cm}^{-2}$ . The peak CH emission reported by Vallée is at the same offset as Kutner's CO observations. Since there is a proportional relationship between  $N(\text{CH})$  and  $N(\text{H}_2)$  (Federman 1982; Danks et al. 1984; Mattila 1986), Vallée inferred that  $N(\text{H}_2) = 2.5 \times 10^{20}$   $\text{cm}^{-2}$ . Vallée used a length of 0.13 pc to convert column density to space density. This length was determined from the fact that the CH abundance extends over 0.3 mag in blue absorption,  $A_B$ . There could easily be a factor of 2 error in this estimate. With this length, Vallée obtained  $n(\text{H}_2) = 600$   $\text{cm}^{-3}$  and then converted  $n(\text{H}_2)$  into a total proton density of  $n = 1300$   $\text{cm}^{-3}$  with the relation  $n = 2.2n(\text{H}_2)$ , assuming that 10% of the gas is He. Vallée's

density, which is similar to ours for  $I_{\text{UV}} = 3$ , may not represent the molecular cloud behind the star as he reported, since his CH abundance is comparable to ours. The molecular material may in fact reside in front of HD 147009. Moreover, this density is similar to densities found in the diffuse component in the reflection nebulae NGC 2023 (this paper) and NGC 7023 (Paper I and this paper).

#### 4.4. *Optical Results for Three Nebulae*

The reflection nebulae NGC 2023 and NGC 7023 are relatively bright extended objects, located at the edges of their respective molecular clouds. For these reasons they have been extensively studied at a variety of wavelengths. The two nebulae have been shown to have clumpy, filamentary structure from infrared observations. The central stars, HD 37903 and HD 200775, of these nebulae have similar spectral types, B1.5 V and B3 Ve, and similar distances of 470 and 430 pc (Perryman et al. 1997), respectively. The peak infrared emission is offset from the stars in both nebulae. As for *vdB 102*, the illuminating source, HD 147009, is of later spectral type (A0 V) and is closer to the Sun at a distance of 160 pc (Perryman et al. 1997). The extent of filamentary structure is unknown.

The physical conditions obtained from optical spectra toward the illuminating stars in the reflection nebulae NGC 2023 and *vdB 102* are similar to those obtained from an earlier study of NGC 7023 (Paper I) and updated here. The physical conditions  $n$ ,  $T$ , and  $I_{\text{UV}}$  inferred for NGC 7023 are 300–900  $\text{cm}^{-3}$ , 40 K, and 1–3, respectively, once the effects of a lower  $x(\text{C}^+)$  are included (Table 10). These physical conditions are similar to those obtained from grain scattering observations of NGC 7023 (Walker et al. 1980; Witt & Cottrell 1980a, 1980b; Witt et al. 1982). The physical conditions found are 500–1500  $\text{cm}^{-3}$ , 40 K, and 1–3 toward NGC 2023 and 400–1200  $\text{cm}^{-3}$ , 40 K, and 1–3 toward *vdB 102* for  $n$ ,  $T$ , and  $I_{\text{UV}}$ , respectively. Therefore, the material in front of the stars in the reflection nebulae NGC 2023, *vdB 102*, and NGC 7023 is relatively diffuse.

In Paper I, an enhancement in the CN abundance over that described in equation (2) was (and is still) needed to explain the observed CN abundance in the foreground PDR of NGC 7023. This enhancement of CN in the foreground material of NGC 7023 is the result of a contribution from dark cloud chemistry (Paper I):  $\text{HCN} \rightarrow \text{CN}$  through photodissociation. If we really are seeing an effect of dark cloud chemistry from the molecular cloud behind the star, the foreground PDR may be closer to the star than our estimates suggest, even for an enhancement by a factor of 3 in the radiation field. This enhancement is not detected toward either HD 37903 or HD 147009, unless the amount of  $\text{C}_2$  in the gas is much less than our current upper limit. This could be a consequence of the different distances between each star and its foreground gas.

In the case of NGC 7023, an hourglass-shaped cavity has been detected (Lemaire et al. 1996; Fuente et al. 1998) around the star. CO radio maps reveal (Gerin et al. 1998) that the  $^{13}\text{CO}$  emission profiles are relatively smooth and centered at 2.5  $\text{km s}^{-1}$  while the  $^{12}\text{CO}$  profiles indicate more complicated structure. This structure shows a gradual shift in the velocity of the gas from 2.5 to 1.5  $\text{km s}^{-1}$ , which is the velocity of the foreground molecular material reported in Paper I. This suggests that there should be a diffuse  $^{12}\text{CO}$  component in the cavity or the foreground material.

We associate this diffuse component with the CO seen in UV absorption. Lemaire et al. (1999) report redshifted H I with respect to H<sub>2</sub> in the molecular cloud behind the star. This trend is also detected in atomic absorption (Paper I), which is blueshifted compared to the foreground molecular material. This is consistent with an expanding PDR around the star (Gerin et al. 1998; Fuente et al. 1998).

The analysis of atomic data provides insight into the processes taking place in the foreground gas. Using the extinction curve for the line of sight in our model, the observed ratio of Na I to K I toward NGC 7023 and vdB 102 matched the predicted ratio. In the cases for  $\zeta$  Per and NGC 2023, the observed ratio was about twice the predicted value. Adjustments to the photoionization rates would bring the predicted ratios into better agreement with observations. In particular, a finer grid for computing the differences in extinction relative to the extinction for  $\zeta$  Per may be more appropriate; we only considered average differences over wavelength regions where the curves intersected. In the comparison of the column density of each species toward the reflection nebulae and  $\zeta$  Per, a small change in  $n_e$  or an extra source of depletion is needed toward NGC 7023 to match the observed and predicted results. Toward HD 147009, a fairly substantial modification is required. A significant increase in  $n_e$ , possibly provided by protons in diffuse ionized gas created by earlier type stars in Sco OB2, is needed to account for the differences found between the nebula vdB 102 and gas toward  $\zeta$  Per.

The analysis of ultraviolet data provides additional pieces to the picture for the gas associated with NGC 2023 and NGC 7023. It appears that the foreground PDR in NGC 7023 is more homogeneous (because C I excitation, C<sub>2</sub> excitation, CO fractionation, and chemical analysis yield very similar physical conditions) and is permeated by a slightly stronger radiation field compared to that for NGC 2023.

## 5. CONCLUSIONS

We presented the first chemical results for foreground material associated with the PDRs of NGC 2023 and

vdB 102. The foreground material in NGC 2023 is more diffuse than the molecular cloud behind HD 37903 and is subjected to a less intense radiation field. The results are similar to what we found for NGC 7023 (Paper I). As for vdB 102, our analyses are the most comprehensive to date and will be the basis for other studies of nebulae illuminated by A-type stars.

Future studies should incorporate details that extend the treatment presented here. The effects of a clumpy distribution of material and a more extensive set of chemical reactions in the framework of a time-dependent model need to be considered. These models have to include the “anomalous” extinction law found for both stars in this work (see also FM90; WBS84). The consequences of NGC 2023 and vdB 102 being located in active star-forming regions are another area for future analysis. Other absorption measurements of species detected at ultraviolet wavelengths, such as H<sub>2</sub>, are needed to place more stringent constraints on physical conditions. Observations with the *Far Ultraviolet Spectroscopic Explorer* will soon be obtained. This combination of visible and UV data on the one hand and more sophisticated modeling efforts on the other will provide a clearer description of the interaction between a star’s radiation field and the surrounding molecular cloud.

We thank David Doss for assistance with the instrumental setups at McDonald Observatory and Tom Ingerson for help with the setup at CTIO. The McDonald Observatory 2dcoudé data presented here formed the basis for the master’s thesis of D. C. K. Tony Imperial and Marissa Lingen helped in reducing CTIO data, and Kyle Westfall reduced the NEWSIPS data for X Per. Marissa and Kyle participated in the Research Experience for Undergraduates (REU) Program at the University of Toledo, which was funded by NSF. We also thank Yaron Sheffer for the use of his code. This research made use of the Simbad database, operated at CDS, Strasbourg, France. This research was supported in part by NASA LTSA grant NAG5-4957.

## APPENDIX A

### RELIABILITY OF NEWSIPS DATA

The *IUE* archive is now comprised of NEWSIPS data, which yields spectra with superior signal-to-noise ratio. Techniques were introduced to perform geometric and photometric corrections, to improve the ripple correction, and to determine the image background (e.g., Nichols 1998). We examined the reliability of our data in two ways. First, we compared our results for another star, 20 Aql, with those of Hanson, Snow, & Black (1992) based on an earlier form of the archive. Then we compared  $W_\lambda$  values of C I lines seen in the *IUE* spectra of X Per with measurements from high-resolution spectra acquired with ECH-A of the Goddard High Resolution Spectrograph on *HST*. Our comparisons show that NEWSIPS data provide a consistent, reliable set of  $W_\lambda$  values with improved signal-to-noise ratio for interstellar studies, thereby confirming the analyses performed by González-Riestra et al. (2000).

Tables 13–15 provide the basis for comparison. Table 13 shows our results for interstellar gas toward 20 Aql based on NEWSIPS data and the results of Hanson et al. (1992). The agreement in  $W_\lambda$  for values from less than 10 to 150 mÅ is excellent, without any discrepancies beyond the mutual uncertainties. The uncertainties associated with the NEWSIPS spectra also tend to be smaller. Sample spectra appear in Figure 11, and Table 14 displays the column densities derived from the fits. In Table 15, NEWSIPS results for C I toward X Per are compared with measurements from ECH-A spectra. Again, the correspondence is excellent. Syntheses of the ECH-A data give a measure of the precision in column density attainable from NEWSIPS data. Since  $b$ -values can be determined from NEWSIPS data to about 0.5 and 0.1 km s<sup>-1</sup> from ECH-A data, column densities from relatively strong lines in NEWSIPS data are accurate to about 50%. This confirms the measure of uncertainty given to atomic column densities in Table 8.

TABLE 13  
UV RESULTS FOR 20 AQUILAE

Absorption Feature	Wavelength (Å)	$f$	$W_{\lambda}(\text{obs})^a$ (mÅ)	$W_{\lambda}(\text{fit})$ (mÅ)	$W_{\lambda}^b$ (mÅ)
$^{12}\text{CO}$ (0–0) .....	1544.448	...	$150 \pm 15$	...	$150 \pm 10$
(1–0) .....	1509.749	0.0291	$113 \pm 11$	109	$115 \pm 5$
(2–0) .....	1477.565	0.0401	$121 \pm 9$	113	$130 \pm 5$
(3–0) .....	1447.352	0.0346	$114 \pm 9$	107	$120 \pm 5$
(4–0) .....	1419.044	0.0233	$106 \pm 8$	96	$110 \pm 6$
(5–0) .....	1392.525	0.0145	$84 \pm 8$	84	$90 \pm 8$
(6–0) .....	1367.623	0.00795	$69 \pm 8$	70	$75 \pm 10$
(7–0) .....	1344.186	0.00414	$59 \pm 8$	57	$63 \pm 6$
(8–0) .....	1322.150	0.00200	$39 \pm 8$	43	$45 \pm 10$
(9–0) .....	1301.403	0.00095	$25 \pm 6$	30	...
(10–0) .....	1281.866	0.00041	$16 \pm 4$	18	...
(11–0) .....	1263.433	0.00018	$12 \pm 4$	10	...
$^{13}\text{CO}$ (1–0) .....	1510.407	0.0351	$97 \pm 9$	...	$95 \pm 6$
(2–0) .....	1478.793	0.0402	$37 \pm 4$	38	$31 \pm 5$
(3–0) .....	1449.145	0.0347	$25 \pm 6$	34	$23 \pm 6$
(4–0) .....	1421.340	0.0242	$29 \pm 5$	27	$25 \pm 8$
(5–0) .....	1395.229	0.0145	$19 \pm 8$	20	$12 \pm 6$
C I ( $J = 0$ ) .....	1276.483	0.00168	$19 \pm 4$	14	$20 \pm 5$
	1280.135	0.0243	$42 \pm 6$	43	$45 \pm 5$
	1328.833	0.0580	$56 \pm 6$	52	$43 \pm 6$
	1560.309	0.0804	$63 \pm 7$	64	$80 \pm 10$
( $J = 1$ ) .....	1276.750	0.00239	$7 \pm 4$	7	$11 \pm 5$
	1279.056	0.00202	$22 \pm 5$	6	$23 \pm 5$
	1279.890	0.0137	$22 \pm 6$	22	$30 \pm 5$
	1280.597	0.00684	$15 \pm 5$	15	$25 \pm 5$
	1329.085	0.0193	$56 \pm 6$	61	$70 \pm 10$
	1560.682	0.0603	$58 \pm 6$	64	$75 \pm 5$
( $J = 2$ ) .....	1277.723	0.0145	$22 \pm 4$	16	$25 \pm 5$
	1277.954	0.000967	$7 \pm 3$	2	$7 \pm 5$
	1279.229	0.00324	$8 \pm 3$	5	$12 \pm 5$
	1279.498	0.000903	$3 \pm 3$	2	$5 \pm 4$
	1280.847	0.00505	$16 \pm 5$	7	$20 \pm 5$
	1329.578	0.0435	$34 \pm 5$	41	$40 \pm 6$
	1561.340	0.0121	$53 \pm 6$	60	$45 \pm 5$
Blends .....	1277.245	0.0967	$98 \pm 7$	87	$120 \pm 10$
	1277.513	0.0242	$68 \pm 5$	62	$60 \pm 8$
	1280.333	0.0147	$32 \pm 6$	27	$30 \pm 8$
S I .....	1295.653	0.087	$31 \pm 8$	21	$20 \pm 10$
	1316.543	0.0381	$31 \pm 8$	24	...
	1425.030	0.141	$27 \pm 6$	24	$20 \pm 8$
	1425.188	0.0269	$16 \pm 4$	17	...
	1472.971	0.0218	$20 \pm 7$	16	...
	1473.994	0.0803	$23 \pm 6$	22	$15 \pm 10$
	1474.379	0.0179	$14 \pm 6$	15	...
	1807.311	0.096	$29 \pm 4$	31	$35 \pm 10$
Ni II .....	1317.217	0.146	$14 \pm 6$	13	$15 \pm 10$
	1370.132	0.144	$12 \pm 5$	14	...
	1741.549	0.0776	$15 \pm 6$	14	$20 \pm 10$

<sup>a</sup> IUE NEWSIPS data.

<sup>b</sup> Hanson et al. 1992.

TABLE 14  
UV COLUMN DENSITIES FOR 20 AQUILAE

Species	$N(\text{fit})$ ( $\text{cm}^{-2}$ )
$N_{\text{tot}}(^{12}\text{CO})$ .....	$(4.3-4.5) \times 10^{15}$
$N_{\text{tot}}(^{13}\text{CO})$ .....	$(1.8-2.0) \times 10^{14}$
$N_{\text{tot}}(\text{C I } (J = 0))$ .....	$(7.2 \pm 2.0) \times 10^{14}$
$N_{\text{tot}}(\text{C I } (J = 1))$ .....	$(2.4 \pm 0.6) \times 10^{14}$
$N_{\text{tot}}(\text{C I } (J = 2))$ .....	$(9.5 \pm 2.7) \times 10^{13}$
$N_{\text{tot}}(\text{S I})$ .....	$(1.1 \pm 0.2) \times 10^{14}$
$N_{\text{tot}}(\text{Ni II})$ .....	$(1.0 \pm 0.4) \times 10^{13}$

TABLE 15  
UV RESULTS FOR X PER

Absorption Feature	Wavelength (Å)	$f$	$W_{\lambda}(\text{GHRs})$ (mÅ)	$W_{\lambda}(\text{fit})$ (mÅ)	$W_{\lambda}(\text{IUE})$ (mÅ)
C I ( $J = 0$ ) .....	1260.734	0.0394	$37.1 \pm 2.7$	39.1	$44.3 \pm 5.5$
	1276.483	0.00168	$28.1 \pm 1.1$	27.4	$29.4 \pm 7.2$
	1277.245	0.0967	$42.0 \pm 1.6$	40.5	$74.6 \pm 6.6^a$
	1280.135	0.0243	$38.1 \pm 1.5$	39.5	$34.6 \pm 6.4$
	1260.927	0.0131	$25.8 \pm 1.8$	25.3	$46.1 \pm 8.1^b$
	1260.996	0.00984	$25.4 \pm 1.8$	24.3	...
	1261.123	0.0164	$27.7 \pm 2.0$	26.5	...
	1276.750	0.00239	$17.0 \pm 0.9$	16.8	$16.8 \pm 4.1$
	1277.282	0.0725	$35.7 \pm 1.3$	36.6	...
	1277.513	0.0242	$26.1 \pm 1.0$	27.1	$49.5 \pm 6.0^c$
1279.056	0.00202	$15.6 \pm 0.9$	15.4	$9.6 \pm 4.1$	
1279.890	0.0137	$26.0 \pm 1.0$	26.7	$20.7 \pm 5.1$	
1280.404	0.00438	$21.5 \pm 0.9$	21.0	$28.9 \pm 5.5$	
1280.597	0.00684	$24.2 \pm 1.0$	23.4	$12.9 \pm 3.8$	
1261.426	0.00984	$11.8 \pm 1.2$	14.5	$35.2 \pm 10.7^d$	
$(J = 2)$ .....	1261.552	0.0295	$20.1 \pm 1.5$	20.0	...
	1277.550	0.0812	$26.3 \pm 1.0$	25.8	$16.1 \pm 5.5$
	1277.723	0.0145	$16.0 \pm 0.9$	17.0	...
	1277.954	0.000967	$2.1 \pm 0.6$	2.7	...
	1279.229	0.00324	$8.7 \pm 0.7$	8.5	...
	1279.498	0.000903	$1.9 \pm 0.6$	2.4	...
	1280.333	0.0147	$17.8 \pm 0.9$	17.3	$34.0 \pm 4.3^e$
	1280.847	0.00505	$10.4 \pm 0.8$	11.1	...

<sup>a</sup> Blend with  $\lambda 1277.282$ .

<sup>b</sup> Blend with  $\lambda 1260.996$ .

<sup>c</sup> Blend with  $\lambda 1277.550$ .

<sup>d</sup> Blend with  $\lambda 1261.552$ .

<sup>e</sup> Blend with  $\lambda 1280.404$ .

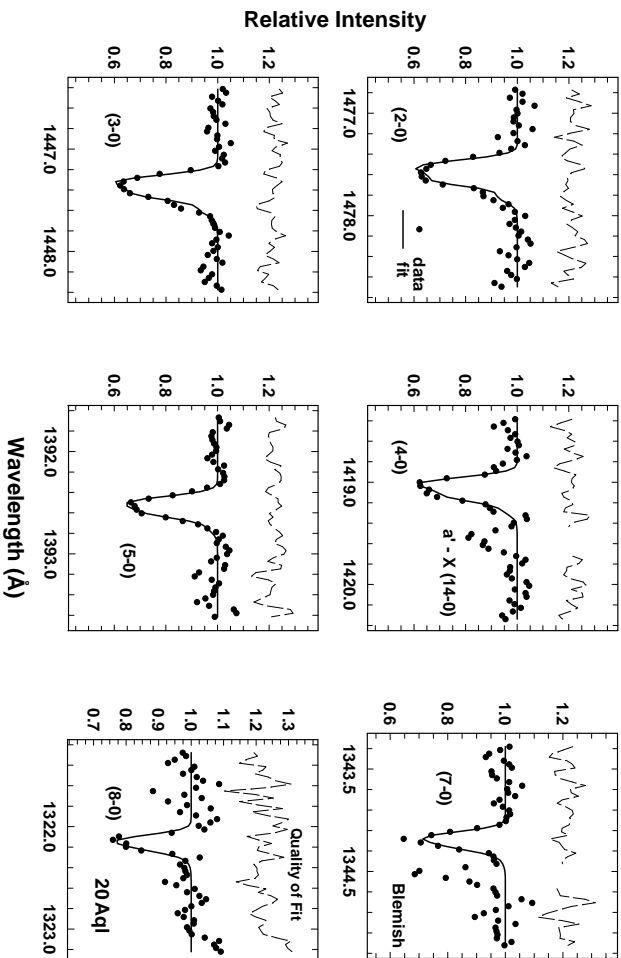


Fig. 11a

Fig. 11—(a) Representative NEWSIPS IUE  $^{13}\text{CO}$  spectra toward 20 Aql. The data are represented by the filled circles. Our best fit to the data (solid line) and the data — fit (dashed line, offset to 1.22) are also displayed. The  $d-X$  (14–0) intersystem band was not fitted. (b) Same as (a), but with spectra of  $^{13}\text{CO}$ . (c) Same as (a), but with spectra of C I, Si I, and Ni II. The Si II line at  $\lambda 1808$  was not fitted. Data — fit offset to 1.30.

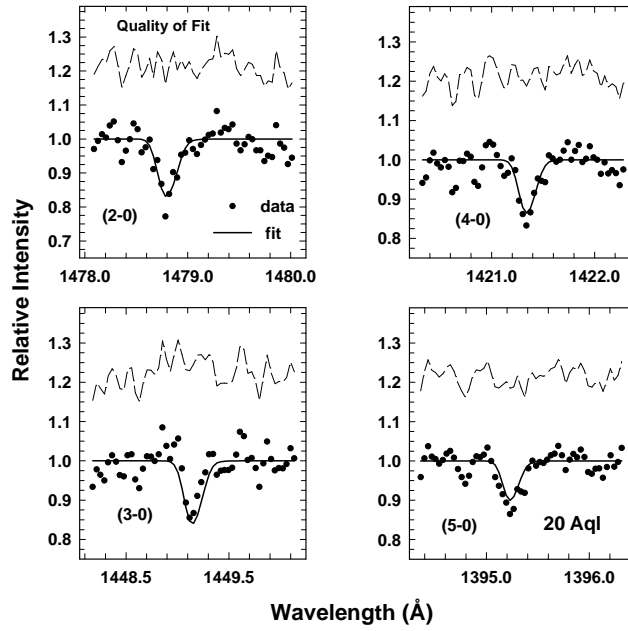


Fig. 11b

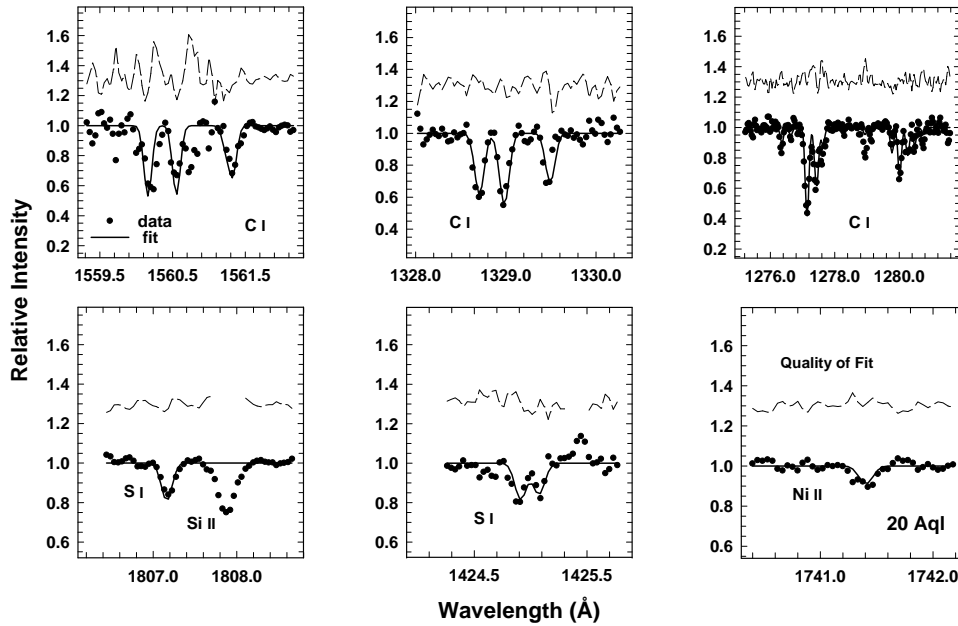


Fig. 11c

For completeness, Tables 16–18 indicate a synthesis of results from ground-based observations of 20 Aql, incorporating data acquired during observing runs described here. This compilation includes the highest resolution spectra taken of 20 Aql. Our spectra are displayed in Figures 12–14. Analyses, similar to those for NGC 2023 and vdB 102, were applied to the data. The density, temperature, and radiation field are  $1400 \text{ cm}^{-3}$ , 50 K, and 1; the factor of 2 increase from Federman, Strom, & Good (1991) in the derived density is due to the lower fractional abundance of carbon. With the exception of the density, the results, derived from the chemical analysis, are much like the results of Federman et al. (1991) and Hanson et al. (1992).

The atomic analysis performed above is repeated for data toward 20 Aql. The inferred Na I and K I photoionization rates are  $3.4 \times 10^{-13}$  and  $1.1 \times 10^{-12} \text{ s}^{-1}$ , which yield a predicted ratio of 54. The observed column densities of  $(1.3 \pm 0.1) \times 10^{15}$  and  $(1.4 \pm 0.1) \times 10^{13} \text{ cm}^{-2}$  for Na I and K I, respectively, produce an observed ratio of  $93 \pm 10$ . The correspondence between observed and predicted  $N(\text{Na I})/N(\text{K I})$  ratios is about 2:1, similar to that found for gas toward  $\zeta$  Per and HD 37903.

For the comparison of the columns Na I and K I of 20 Aql to those of  $\zeta$  Per, the total proton density toward 20 Aql is needed. The proton density is  $(3.0 \pm 0.6) \times 10^{21} \text{ cm}^{-2}$  (Hanson et al. 1992) with an assumed 20% error (see text above). This results in a predicted ratio  $N(\text{Na I})_{20 \text{ Aql}}/N(\text{Na I})_{\zeta \text{ Per}}$  of  $29 \pm 8$  and  $36 \pm 10$  for K I. The observed ratios are  $18 \pm 2$  for Na I and  $19 \pm 2$  for K I. The effect of  $\alpha_c$  was not needed in this analysis (see text above). Formally, the predicted and observed ratios are consistent with (at most) a modest change in  $n_e$  and/or depletion to bring the predictions into better agreement with the observations, much like the results for the PDR toward HD 200775.

TABLE 16  
GROUND-BASED RESULTS FOR 20 AQUILAE

SPECIES	WAVELENGTH (Å)	McD (MODERATE RES) <sup>a</sup>		McD (HIGH RES) <sup>a</sup>		McD (HIGH RES) <sup>b</sup>		CTIO (MODERATE RES)		OTHER
		$W_{\lambda}$ (mÅ)	$v_{\text{LSR}}$ (km s <sup>-1</sup> )	$W_{\lambda}$ (mÅ)	$v_{\text{LSR}}$ (km s <sup>-1</sup> )	$W_{\lambda}$ (mÅ)	$v_{\text{LSR}}$ (km s <sup>-1</sup> )	$W_{\lambda}$ (mÅ)	$v_{\text{LSR}}$ (km s <sup>-1</sup> )	$W_{\lambda}$ (mÅ)
CH .....	4300.313	13.0±0.2	3.8	13.3±0.3	2.8	14.2±0.7	2.4	14.3±0.6	3.3	12.6±1.3 <sup>c</sup>
	3878.774	1.5±0.2	1.4	...	...	...	...	...	...	...
	3886.409	4.0±0.3	1.6	...	...	...	...	3.1±0.8	0.9	...
	3890.217	3.0±0.3	2.1	...	...	...	...	≤2.3	...	...
CH <sup>+</sup> .....	4232.548	2.8±0.2	4.0	2.6±0.3	1.3	2.8±0.3	5.0	2.6±0.7	0.2	3.3±0.8 <sup>c</sup>
	3957.692	1.7±0.2	2.6	...	...	...	...	2.9±1.4	0.2	...
CN .....	3874.00	3.2±0.2	1.3	3.2±0.3	2.3	...	...	≤3.7	...	...
	3874.61	11.5±0.2	0.7	11.3±0.3	2.2	...	...	13.4±2.3	1.1	10.0±2.0 <sup>c</sup>
	3875.76	1.6±0.2	0.6	1.7±0.3	2.5	...	...	≤3.7	...	...
Ca II .....	3968.468	2.9±0.7	-15.0	...	...	...	...	5.5±3.4	-20.4	...
		13.4±0.5	-8.9	...	...	...	...	28.9±4.3	-8.6	...
		61.5±0.7	0.9	...	...	...	...	62.3±3.8	0.7	...
	3933.663	3.4±0.9	-18.5	5.9±1.1	-14.0	4.6±0.7	-15.6	4.6±1.1	-18.3	...
		32.6±0.8	-7.9	25.2±0.2	-7.7	24.7±0.6	-8.4	43.5±2.4	-9.2	...
		...	...	33.8±0.8	-0.2	...	...	82.0±2.2	0.1	...
		85.2±0.8	2.1	37.2±0.8	2.8	77.0±1.2	1.3	...	...	...
Ca I .....	4226.728	0.8±0.1	-5.4	0.7±0.1	-7.3	...	...	...	...	...
		4.2±0.2	3.5	3.7±0.2	1.7	2.9±0.3	2.9	2.1±0.5	3.5	4.0±0.2 <sup>c</sup>
Na I .....	5895.924	89.0±35.8	-8.0	...	...	78.0±1.0	-7.7	...	...	...
		210.6±43.6	2.4	...	...	186.0±2.0	2.3	...	...	...
	5889.951	94.8±28.5	-8.1	...	...	...	...	...	...	...
K I .....	7698.974	244.4±41.0	2.4	...	...	...	...	...	...	...
		6.2±1.3	-8.9	...	...	4.5±0.6	-7.8	...	...	...
		111.3±1.4	2.6	...	...	110.0±1.0	1.5	...	...	...

<sup>a</sup> 2dcoudé.

<sup>b</sup> 6 foot camera.

<sup>c</sup> Hanson et al. 1992.

TABLE 17  
C<sub>2</sub> DATA TOWARD 20 AQUILAE

Line	$\lambda$ (Å)	$W_{\lambda}$ (mÅ)	$V_{\text{LSR}}$ (km s <sup>-1</sup> )	$N$ (cm <sup>-2</sup> )	Notes
R(0) .....	8757.69	2.0±1.0	7.4	(3.0±1.5) × 10 <sup>12</sup>	a
		2.0±0.2	...	(3.0±0.3) × 10 <sup>12</sup>	b
N(0) .....	8766.03	≤1.1	...	(3.0±0.3) × 10 <sup>12</sup>	c
P(2) .....		≤1.6	...	≤1.6 × 10 <sup>13</sup>	b
Q(2) .....	8761.19	3.9±0.5	7.2	(1.2±0.2) × 10 <sup>13</sup>	a
		7.3±0.5	...	(2.3±0.2) × 10 <sup>13</sup>	b
R(2) .....	8753.95	3.4±0.7	6.8	(1.3±0.4) × 10 <sup>13</sup>	a
		5.0±0.4	...	(1.9±0.2) × 10 <sup>13</sup>	b
N(2) .....	8773.43	1.8±0.3	...	(1.8±0.1) × 10 <sup>13</sup>	c
P(4) .....		1.6±0.3	...	(1.6±0.3) × 10 <sup>13</sup>	b
Q(4) .....	8763.75	3.3±0.4	7.8	(9.9±1.3) × 10 <sup>12</sup>	a
		5.7±0.5	...	(1.8±0.2) × 10 <sup>13</sup>	b
R(4) .....	8751.68	3.1±1.4	5.2	(1.3±0.3) × 10 <sup>13</sup>	a
		3.2±0.2	...	(1.5±0.1) × 10 <sup>13</sup>	b
N(4) .....	8782.31	1.8±0.3	...	(1.4±0.1) × 10 <sup>13</sup>	c
P(6) .....		3.1±0.6	...	(2.4±0.5) × 10 <sup>13</sup>	b
Q(6) .....	8767.76	4.6±1.6	8.5	(1.4±0.5) × 10 <sup>13</sup>	a
		4.2±0.4	...	(1.3±0.1) × 10 <sup>13</sup>	b
R(6) .....	8750.85	≤5.0	...	≤2.5 × 10 <sup>13</sup>	a
		3.0±0.3	...	(1.5±0.2) × 10 <sup>13</sup>	b
N(6) .....	8773.22	1.8±0.3	...	(1.4±0.1) × 10 <sup>13</sup>	c
Q(8) .....		≤1.8	...	≤5.4 × 10 <sup>12</sup>	a
N(8) .....		1.1±0.3	...	(3.3±0.9) × 10 <sup>12</sup>	b
		...	...	(3.3±0.9) × 10 <sup>12</sup>	c
$N_{\text{tot}}(\text{C}_2)$ .....				(5.2±1.6) × 10 <sup>13</sup>	d

<sup>a</sup>  $b = 1.0 \text{ km s}^{-1}$ .

<sup>b</sup> Federman et al. 1994.

<sup>c</sup> Weighted average of individual detections.

<sup>d</sup> Sum of the weighted averages of the 0, 2, 4, 6, and 8 rotational lines.

TABLE 18  
COLUMN DENSITIES FOR 20 AQUILAE

Species	Wavelength (Å)	$v_{LSR}$ (km s <sup>-1</sup> )	$N_{obs}^{a,b}$ (cm <sup>-2</sup> )
$N(\text{CH})$ .....	4300.313	3.0	$(2.0 \pm 0.1) \times 10^{13}$
	3878.774	1.4	$(1.1 \pm 0.1) \times 10^{13}$
	3886.409	1.6	$(9.4 \pm 0.7) \times 10^{12}$
	3890.217	2.1	$(1.1 \pm 0.1) \times 10^{13}$
$N_{tot}(\text{CH})$ .....	...	...	$(2.0 \pm 0.1) \times 10^{13}$
$N(\text{CH}^+)$ .....	4232.548	2.3	$(3.2 \pm 0.2) \times 10^{12}$
	3957.692	1.7	$(3.8 \pm 0.5) \times 10^{12}$
$N_{tot}(\text{CH}^+)$ .....	...	...	$(3.3 \pm 0.2) \times 10^{12}$
$N(\text{CN})$ .....	3874.00	1.8	$(1.1 \pm 0.1) \times 10^{12}$
	3874.61	1.3	$(3.1 \pm 0.1) \times 10^{12}$
	3875.76	2.1	$(1.1 \pm 0.1) \times 10^{12}$
$N_{tot}(\text{CN})$ .....	...	...	$(4.2 \pm 0.1) \times 10^{12}$
$N(\text{Ca II H})$ .....	3968.468	-17.7	$(2.3 \pm 0.7) \times 10^{11}$
$N(\text{Ca II K})$ .....	3933.663	-16.6	$(4.8 \pm 0.1) \times 10^{11}$
$N_{-17}(\text{Ca II})$ .....	...	...	$(4.8 \pm 0.1) \times 10^{11}$
$N(\text{Ca II H})$ .....	3968.468	-8.8	$(3.4 \pm 0.1) \times 10^{11}$
$N(\text{Ca II K})$ .....	3933.663	-8.3	$(3.6 \pm 0.1) \times 10^{11}$
$N_{-8}(\text{Ca II})$ .....	...	...	$(3.5 \pm 0.1) \times 10^{11}$
$N(\text{Ca II H})$ .....	3968.468	0.8	$(2.4 \pm 0.1) \times 10^{11}$
$N(\text{Ca II K})$ .....	3933.663	-0.2	$(5.0 \pm 0.2) \times 10^{11}$
$N_0(\text{Ca II})$ .....	...	...	$(2.9 \pm 0.1) \times 10^{11}$
$N_1(\text{Ca II K})$ .....	3933.663	1.2	$(2.2 \pm 0.1) \times 10^{12}$
$N_3(\text{Ca II K})$ .....	...	2.8	$(5.6 \pm 0.2) \times 10^{11}$
$N_7(\text{Ca II K})$ .....	...	7.3	$(1.2 \pm 0.1) \times 10^{11}$
$N_{-7}(\text{Ca I})$ .....	4226.728	-7.3	$(2.8 \pm 0.3) \times 10^9$
$N_3(\text{Ca I})$ .....	...	2.9	$(1.4 \pm 0.1) \times 10^{10}$
$N(\text{Na I D}_1)$ .....	5895.924	-8.0	$(1.0 \pm 0.1) \times 10^{13}$
$N(\text{Na I D}_2)$ .....	5889.951	-8.1	$(1.8 \pm 4.0) \times 10^{13}$
$N_{-8}(\text{Na I})$ .....	...	...	$(1.0 \pm 0.1) \times 10^{13}$
$N(\text{Na I D}_1)$ .....	5895.924	2.4	$(1.4 \pm 0.1) \times 10^{15}$
$N(\text{Na I D}_2)$ .....	5889.951	2.4	$(7.3 \pm 3.0) \times 10^{14}$
$N_3(\text{Na I})$ .....	...	...	$(1.3 \pm 0.1) \times 10^{15}$
$N_{-9}(\text{K I})$ .....	7698.974	-8.9	$(2.8 \pm 0.4) \times 10^{10}$
$N_3(\text{K I})$ .....	...	2.6	$(1.4 \pm 0.1) \times 10^{13}$

<sup>a</sup> Column densities determined from weighted average of detections.

<sup>b</sup>  $b = 1.0 \text{ km s}^{-1}$  for CH, CN, Ca I, Na I, and K I and  $2.5 \text{ km s}^{-1}$  for CH<sup>+</sup> and Ca II.

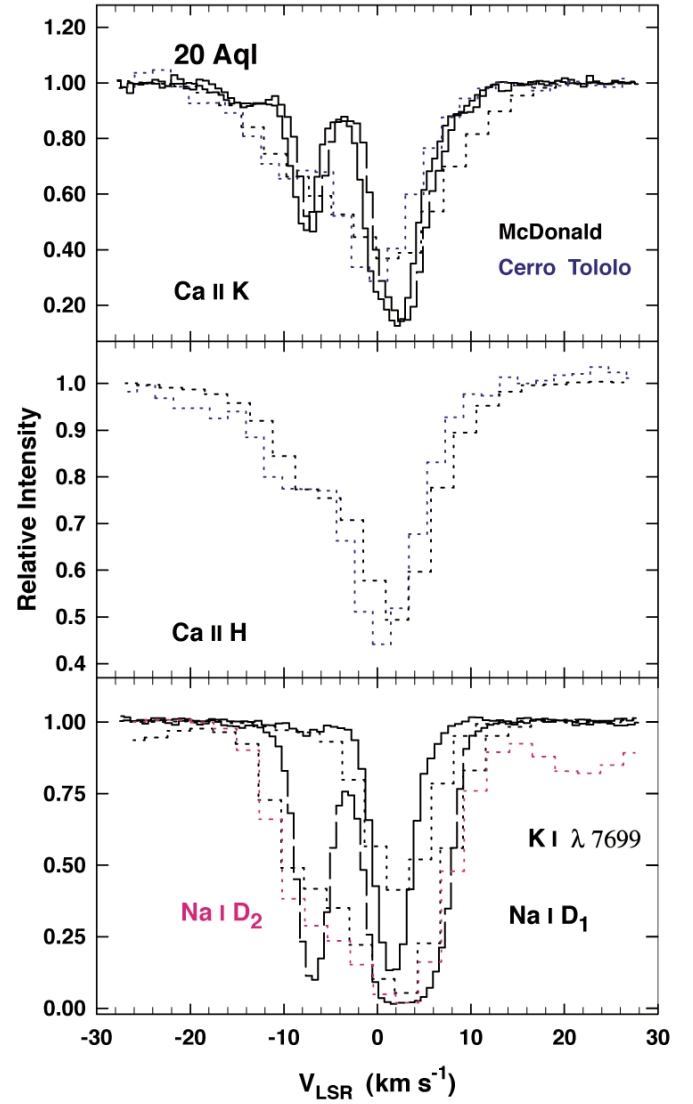


FIG. 12.—Representative atomic spectra toward 20 Aql. *Top*: Ca II K; thick solid line is high-resolution 6 foot camera data, thick long-dashed line is high-resolution 2dcoudé data, thick dashed line is moderate-resolution 2dcoudé data, and blue dashed line is moderate-resolution CTIO data. *Middle*: Ca II H; thick dashed line is moderate-resolution 2dcoudé data, and blue dashed line is moderate-resolution CTIO data. *Bottom*: Spectra of several atomic species taken with different instruments at different resolutions. There is excellent agreement among all observations. Solid line is K I and thick long-dashed line is Na D<sub>1</sub> high-resolution 6 foot camera data; saturated thick dashed line is moderate-resolution 2dcoudé Na D<sub>1</sub> data while weaker thick dashed line is K I; and pink dashed line is moderate-resolution 2dcoudé Na D<sub>2</sub> data.

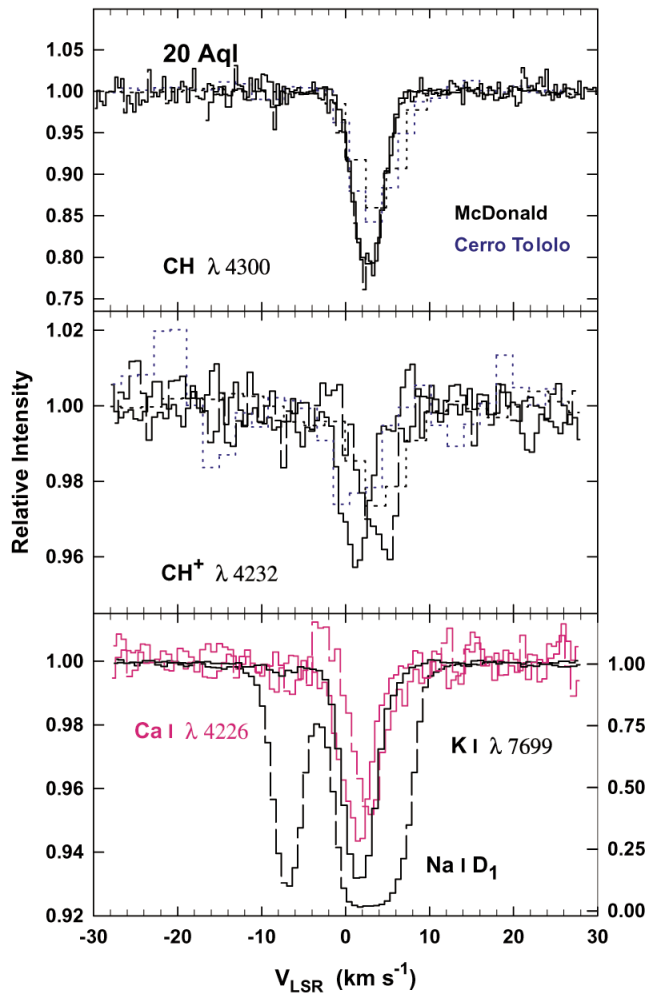


FIG. 13.—Representative spectra toward 20 Aql. *Top*: CH; thick solid line is high-resolution 2dcoué data, thick long-dashed line is the high-resolution 6 foot camera data, thick dashed line is moderate-resolution 2dcoué data, and blue dashed line is moderate resolution CTIO data. *Middle*: CH<sup>+</sup>; solid line is high-resolution 2dcoué data, thick long-dashed line is the high-resolution 6 foot camera data, thick dashed line is moderate-resolution 2dcoué data, and blue dashed line is moderate-resolution CTIO data. *Bottom*: Spectra of several atomic species taken with different instruments at different resolutions. There is excellent agreement among all observations. Solid pink line is Ca I high-resolution 2dcoué data, pink and thick long-dashed lines show Ca I and Na D<sub>1</sub> high-resolution 6 foot camera data, and thick solid line is K I high-resolution 6 foot camera data. Use the right scale for Na I and K I and the left scale for Ca I.

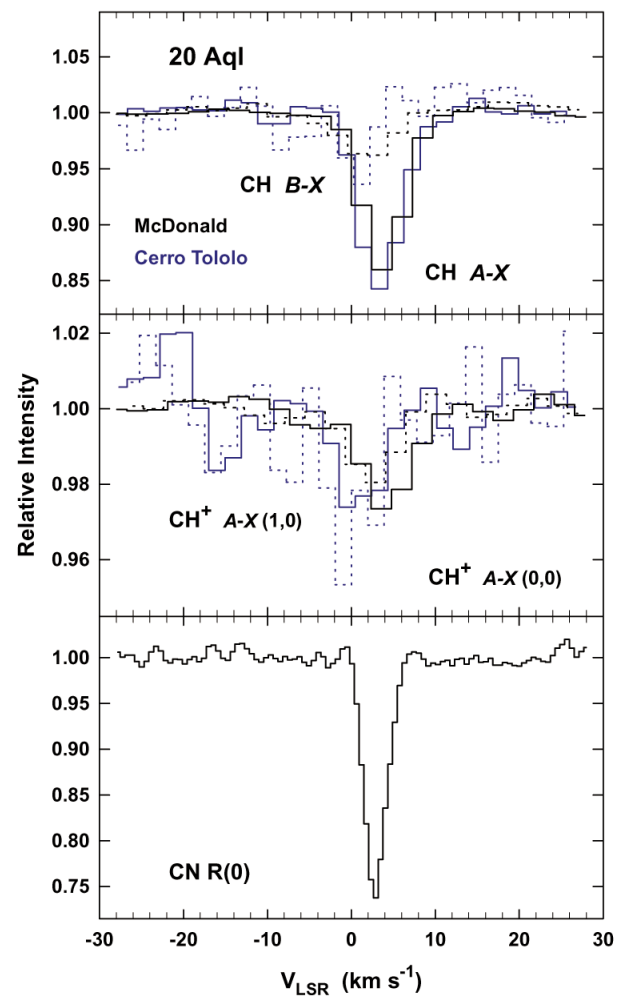


FIG. 14.—Moderate-resolution molecular spectra toward 20 Aql; thick lines are 2dcoué data, and blue lines are CTIO data. *Top*: CH; solid lines are A-X transition, and dashed lines are B-X transition. *Middle*: CH<sup>+</sup>; solid lines are A-X (0-0) transition, and dashed lines are A-X (1-0) transition. *Bottom*: CN R(0) high-resolution 2dcoué data.

## REFERENCES

- Allen, M. M. 1994, *ApJ*, 424, 754  
 Bally, J., & Langer, W. D. 1982, *ApJ*, 255, 143  
 Bertoldi, F., & Draine, B. T. 1996, *ApJ*, 458, 222  
 Bohlin, R. C., Savage, B. D., & Drake, J. F. 1978, *ApJ*, 224, 132  
 Burton, M. G., Howe, J. E., Geballe, T. R., & Brand, P. W. J. L. 1998, *Publ. Astron. Soc. Australia*, 15, 194  
 Buss, R. H., Jr., Allen, M., McCandliss, S., Kruk, J., Liu, J., & Brown, T. 1994, *ApJ*, 430, 630  
 Cappa de Nicolau, C. E., & Pöppel, W. G. L. 1986, *A&A*, 164, 274  
 Cardelli, J. A., Clayton, G. C., & Mathis, J. S. 1989, *ApJ*, 345, 245 (CCM89)  
 Chaffee, F. H., Jr., & White, R. E. 1982, *ApJS*, 50, 169  
 Cowie, L. L., Songaila, A., & York, D. G. 1979, *ApJ*, 230, 469  
 Crutcher, R. M. 1975, *ApJ*, 202, 634  
 Danks, A. C., Federman, S. R., & Lambert, D. L. 1984, *A&A*, 130, 62  
 de Geus, E. J., & Burton, W. B. 1991, *A&A*, 246, 559  
 de Geus, E. J., de Zeeuw, P. T., & Lub, J. 1989, *A&A*, 216, 44 (ddL89)  
 Draine, B. T. 1978, *ApJS*, 36, 595  
 Draine, B. T., & Bertoldi, F. 1996, *ApJ*, 468, 269

- Draine, B. T., & Bertoldi, F. 1999, in *ESA-SP 427, The Universe as Seen by ISO*, ed. P. Cox & M. F. Kessler (Noordwijk: ESA), 783  
 Eggen, O. J. 1998, *AJ*, 116, 1314  
 Federman, S. R. 1982, *ApJ*, 257, 125  
 Federman, S. R., & Cardelli, J. A. 1995, *ApJ*, 452, 269  
 Federman, S. R., Danks, A. C., & Lambert, D. L. 1984, *ApJ*, 287, 219  
 Federman, S. R., Glassgold, A. E., & Kwan, J. 1979, *ApJ*, 227, 466  
 Federman, S. R., & Huntress, W. T., Jr. 1989, *ApJ*, 338, 140  
 Federman, S. R., Knauth, D. C., Lambert, D. L., & Andersson, B.-G. 1997, *ApJ*, 489, 758 (Paper I)  
 Federman, S. R., & Lambert, D. L. 1988, *ApJ*, 328, 777  
 Federman, S. R., Strom, C. J., & Good, J. C. 1991, *AJ*, 102, 1393  
 Federman, S. R., Strom, C. J., Lambert, D. L., Cardelli, J. A., Smith, V. V., & Joseph, C. L. 1994, *ApJ*, 424, 772  
 Field, D., Gerin, M., Leach, S., Lemaire, J. L., Pineau des Forêts, G., Rostas, F., Rouan, D., & Simons, D. 1994, *A&A*, 286, 909  
 Field, D., Lemaire, J. L., Pineau des Forêts, G., Gerin, M., Leach, S., Rostas, F., & Rouan, D. 1998, *A&A*, 333, 280



- Fitzpatrick, E. L., & Massa, D. 1990, *ApJS*, 72, 163 (FM90)
- Freyberg, M. J., & Schmitt, J. H. M. M. 1995, *A&A*, 296, L21
- Fuente, A., Martín-Pintado, J., Cernicharo, J., & Bachiller, R. 1993, *A&A*, 276, 473
- Fuente, A., Martín-Pintado, J., & Gaume R. 1995, *ApJ*, 442, L33
- Fuente, A., Martín-Pintado, J., Rodríguez-Franco, A., & Moriarty-Schieven, G. D. 1998, *A&A*, 339, 575
- Gatley, I., et al. 1987, *ApJ*, 318, L73
- Gerin, M., Phillips, T. G., Keene, J., Betz, A. L., & Boreiko, R. T. 1998, *ApJ*, 500, 329
- Gonzalez-Riestra, R., Cassatella, A., Solano, E., Altamore, A., & Wamsteker, W. 2000, *A&AS*, 141, 343
- Gredel, R., van Dishoeck, E. F., & Black, J. H. 1993, *A&A*, 269, 477
- Hanson, M. M., Snow, T. P., & Black, J. H. 1992, *ApJ*, 392, 571
- Harvey, P. M., Thronson, H. A., Jr., & Gatley, I. 1980, *ApJ*, 235, 894
- Hobbs, L. M. 1974a, *ApJ*, 188, L67
- . 1974b, *ApJ*, 191, 381
- Hollenbach, D., & Natta, A. 1995, *ApJ*, 455, 133
- Hollenbach, D. J., Takahashi, T., & Tielens, A. G. G. M. 1991, *ApJ*, 377, 192
- Hollenbach, D. J., & Tielens, A. G. G. M. 1999, *Rev. Mod. Phys.*, 71, 173 (HT99)
- Hudson, R. D., & Carter, V. L. 1965, *Phys. Rev.*, 139, 1426
- . 1967a, *J. Opt. Soc. Am.*, 57, 651
- . 1967b, *J. Opt. Soc. Am.*, 57, 1471
- Israel, F. P. 1978, *A&A*, 70, 769
- Jaffe, D. T., Genzel, R., Harris, A. I., Howe, J. E., Stacey, G. J., & Stutzki, J. 1990, *ApJ*, 353, 193
- Joseph, C. L., Snow, T. P., Jr., Seab, C. G., & Crutcher, R. M. 1986, *ApJ*, 309, 771
- Knauth, D. C., Federman, S. R., Lambert, D. L., & Crane, P. 2000, *Nature*, 405, 656
- Kutner, M. L., Machnik, D. E., Tucker, K. D., & Dickman, R. L. 1980, *ApJ*, 237, 734
- Lada, E. A., DePoy, D. L., Evans, N. J., II, & Gatley, I. 1991, *ApJ*, 371, 171
- Lambert, D. L., Sheffer, Y., Gilliland, R. L., & Federman, S. R. 1994, *ApJ*, 420, 756
- Lavendy, H., Robbe, J. M., & Gandara, G. 1987, *J. Phys. B*, 20, 3067
- Lebrón, M., & Rodríguez, L. F. 1997, *Rev. Mexicana Astron. Astrofis.*, 33, 165
- Lemaire, J. L., Field, D., Gerin, M., Leach, S., Pineau des Forêts, G., Rostas, F., & Rouan, D. 1996, *A&A*, 308, 895
- Lemaire, J. L., Field, D., Maillard, J. P., Pineau des Forêts G., Falgarone, E., Pijpers, F. P., Gerin, M., & Rostas, F. 1999, *A&A*, 349, 253
- Malin, D. F., Ogura, K., & Walsh, J. R. 1987, *MNRAS*, 227, 361
- Marr, G. V., & Creek, D. M. 1968, *Proc. R. Soc. London A*, 304, 233
- Martini, P., Sellgren, K., & DePoy, D. L. 1999, *ApJ*, 526, 772
- Mattila, K. 1986, *A&A*, 160, 157
- Meixner, M., & Tielens, A. G. G. M. 1993, *ApJ*, 405, 216
- Messing, I., Filseth, S. V., Sadowski, C. M., & Carrington, T. 1981, *J. Chem. Phys.*, 74, 3874
- Meyer, D. M., Cardelli, J. A., & Sofia, U. J. 1997, *ApJ*, 490, L103
- Meyer, D. M., Jura, M., & Cardelli, J. A. 1998, *ApJ*, 493, 222
- Meyer, D. M., & Roth, K. C. 1991, *ApJ*, 376, L49
- Morton, D. C. 1991, *ApJS*, 77, 119
- Morton, D. C., & Noreau, L. 1994, *ApJS*, 95, 301
- Nichols, J. S. 1998, in *ESA SP-413, Ultraviolet Astronomy beyond the IUE Final Archive*, ed. W. Wamsteker & R. González-Riestra (Noordwijk: ESA), 671
- Pankonin, V., & Walmsley, C. M. 1976, *A&A*, 48, 341
- . 1978, *A&A*, 67, 129
- Péquignot, D., & Aldrovandi, S. M. V. 1986, *A&A*, 161, 169
- Perryman, M. A. C., et al. 1997, *A&A*, 323, L49
- Phillips, A. P., Pettini, M., & Gondhalekar, P. M. 1984, *MNRAS*, 206, 337
- Pouilly, B., Robbe, J. M., Schamps, J., & Roueff, E. 1983, *J. Phys. B*, 16, 437
- Racine, R. 1968, *AJ*, 73, 233
- Rogers, C., Heyer, M. H., & Dewdney, P. E. 1995, *ApJ*, 442, 694
- Rouan, D., Field, D., Lemaire, J. L., Lai, O., Pineau des Forêts, G., Falgarone, E., & Deltorn, J. M. 1997, *MNRAS*, 284, 395
- Sandner, W., Gallagher, T. F., Safinya, K. A., & Gounard, F. 1981, *Phys. Rev. A*, 23, 2732
- Savage, B. D., Massa, D., Meade, M., & Wesselius, P. R. 1985, *ApJS*, 59, 397
- Savage, B. D., & Mathis, J. S. 1979, *ARA&A*, 17, 73
- Schmatjko, K. J., & Wolfrum, J. 1976, 16th Symp. (International) on Combustion (Pittsburgh: The Combustion Institute), 819
- Sofia, U. J., Cardelli, J. A., Guerin, K. P., & Meyer, D. M. 1997, *ApJ*, 482, L105
- Steiman-Cameron, T. Y., Haas, M. R., Tielens, A. G. G. M., & Burton, M. G. 1997, *ApJ*, 478, 261
- Strom, K. S., Strom, S. E., Carrasco, L., & Vrba, F. J. 1975, *ApJ*, 196, 489
- Takami, M., Usuda, T., Sugai, H., Kawabata, H., Suto, H., & Tanaka, M. 2000, *ApJ*, 529, 268
- Tielens, A. G. G. M., & Hollenbach, D. 1985a, *ApJ*, 291, 722
- . 1985b, *ApJ*, 291, 747
- Tull, R. G., MacQueen, P. J., Sneden, C., & Lambert, D. L. 1995, *PASP*, 107, 251
- Vallée, J. P. 1987, *Ap&SS*, 137, 217
- van den Bergh, S. 1966, *AJ*, 71, 990
- van Dishoeck, E. F. 1987, in *IAU Symp. 120, Astrochemistry*, ed. M. S. Vardya & S. P. Tarafdar (Dordrecht: Reidel), 51
- van Dishoeck, E. F., & Black, J. H. 1986, *ApJS*, 62, 109
- . 1988, *ApJ*, 334, 771
- Walker, G. A. H., Yang, S., Fahlman, G. G., & Witt, A. N. 1980, *PASP*, 92, 411
- Watson, W. D., Anicich, V. G., & Huntress, W. T., Jr. 1976, *ApJ*, 205, L165
- Welty, D. E., & Hobbs, L. M. 2001, *ApJS*, 133, 345
- Welty, D. E., Hobbs, L. M., & Kulkarni, V. P. 1994, *ApJ*, 436, 152
- Welty, D. E., Morton, D. C., & Hobbs, L. M. 1996, *ApJS*, 106, 533
- Witt, A. N., Bohlin, R. C., & Stecher, T. P. 1981, *ApJ*, 244, 199
- . 1984, *ApJ*, 279, 698 (WBS84)
- Witt, A. N., & Cottrell, M. J. 1980a, *AJ*, 85, 22
- . 1980b, *ApJ*, 235, 899
- Witt, A. N., Walker, G. A. H., Bohlin, R. C., & Stecher, T. P. 1982, *ApJ*, 261, 492
- Wyrowski, F., Walmsley, C. M., Goss, W. M., & Tielens, A. G. G. M. 2000, *ApJ*, 543, 245
- Wyrowski, F., Walmsley, C. M., & Tielens, A. G. G. M. 1997, *A&A*, 324, 1135
- Zsargó, J., & Federman, S. R. 1998, *ApJ*, 498, 256
- Zsargó, J., Federman, S. R., & Cardelli, J. A. 1997, *ApJ*, 484, 820
- Zuckerman, B. 1973, *ApJ*, 183, 863

*Note added in proof.*—The rate constants determined in our earlier work (Federman & Huntress 1989; Federman et al. 1994) were based on *rates* needed to bring predictions into agreement with observations. When lowering the elemental abundance of carbon, as was done in the present paper, without compensating with a larger rate constant, the important rates are altered. The rate constants  $k_1$  and  $k_5$  need to be increased to  $5.4 \times 10^{-10}$  and  $5.0 \times 10^{-10} \text{ cm}^3 \text{ s}^{-1}$ , respectively, in order to keep the rates the same. The changes in  $x(\text{O})$  and  $x(\text{N})$  are too small to affect estimated rates in a significant way.

Returning the rates to their previous values changes the gas density and scale lengths inferred here in the following way. In order to realize similar predicted molecular column densities,  $n$  derived from the chemical analysis must be decreased by about 50%. Use of lower densities leads to closer correspondence with our earlier results on HD 200775 (Federman et al. 1997) and 20 Aql (Federman et al. 1991). The atomic results (predicted column density ratios) are essentially unchanged by the revised values for  $n$  because ratios are used in this analysis. Lower densities also increase  $I_{\text{uv}}/n$  in Table 12 by a factor of 2, but the PDRs still represent a small portion (3%–5%) of the total column. Finally, the analysis of PDR and cloud sizes from equation (6) remains consistent with the results from  $I_{\text{uv}}/n$ : while both sizes increase for a lower  $n$ , the PDR fraction is 1%–3%.